The Canadian Journal of Chemical Engineering

formerly

CANADIAN JOURNAL OF TECHNOLOGY

CONTENTS

Effect of Natural Convection on Transition to Turbulence in Vertical Pipes	*George F. Scheele, Edward M. Rosen, Thomas J. Hanratty*	67
Critical Velocity of Gas	*A. P. Buthod, Chi Tien*	74
Salt Effect in Vapor-Liquid Equilibrium, Part II	*A. I. Johnson, W. F. Furter*	78
Erratum	*G. L. Osberg*	87
Solvent Extraction of Saskatchewan Lignites. II Note on the Properties of the Extract	*S. D. Cavers, R. L. Eager, J. H. Hudson*	88
Polymeric Self-Sealing Distillation and Extractor Trays	*J. D. Kilgallon, H. R. L. Streight*	89

Published by
THE CHEMICAL INSTITUTE OF CANADA
OTTAWA CANADA

The Canadian Journal of Chemical Engineering

formerly

Canadian Journal of Technology

VOLUME 38 JUNE, 1960 NUMBER 3

Authorized as second class mail, Post Office Department, Ottawa. Printed in Canada

Manuscripts for publication should be submitted to the Editor: Dr. A. Cholette, Faculty of Science, Laval University, Boulevard de l'Entente, Quebec, Que. (Instructions to authors are on the next page).

Editorial, Production and Circulation Offices: 48 Rideau Street, Ottawa 2, Ont.

Advertising Office: C. N. McCuaig, manager of advertising sales, *The Canadian Journal of Chemical Engineering*, Room 601, 217 Bay Street, Toronto, Ont. Telephone—EMpire 3-3871.

Plates and Advertising Copy: Send to *The Canadian Journal of Chemical Engineering*, 48 Rideau Street, Ottawa 2, Ont.

Subscription Rates: In Canada—$6.00 per year and $1.25 per single copy; U.S. and U.K.—$7.00, Foreign—$7.50.

Change of Address: Advise Circulation Department in advance of change of address, providing old as well as new address. Enclose address label if possible.

The Canadian Journal of Chemical Engineering is published by The Chemical Institute of Canada every two months.

The Canadian Journal of Chemical Engineering

INSTRUCTIONS TO AUTHORS

Manuscript Requirements for Articles

1. The manuscript should be in English or French.
2. The original and two copies of the manuscript should be supplied. These are to be on 8½ x 11 inch sheets, typewritten, and double spaced. Each page should be numbered.
3. Symbols should conform to American Standards Association. An abridged set of acceptable symbols is found in the third edition of Perry's Chemical Engineers' Handbook. Greek letters and subscripts and superscripts should be carefully made.
4. Abstracts of not more than 200 words in English indicating the scope of the work and the principal findings should accompany all technical papers.
5. References should be listed in the order in which they occur in the paper, after the text, using the form shown here: "Othmer, D. F., Jacobs, Jr., J. J., and Levy, J. F., Ind. Eng. Chem. **34**, 286 (1942). Abbreviations of journal names should conform to the "List of Periodicals Abstracted by Chemical Abstracts". Abbreviations of the common journals are to be found in Perry's Handbook also. All references should be carefully checked with the original article.
6. Tables should be numbered in Arabic numerals. They should have brief descriptive titles and should be appended to the paper. Column headings should be brief. Tables should contain a minimum of descriptive material.
7. All figures should be numbered from 1 up, in Arabic numerals. Drawings should be carefully made with India ink on white drawing paper or tracing linen. All lines should be of sufficient thickness to reproduce well, especially if the figure is to be reduced. Letters and numerals should be carefully and neatly made, with a stencil. Generally speaking, originals should not be more than twice the size of the desired reproduction; final engravings being 3¼ in. or 7 in. wide depending on whether one column or two is used.
8. Photographs should be made on glossy paper with strong contrasts. Photographs or groups of photographs should not be larger than three times the size of the desired reproduction.
9. All tables and figures should be referred to in the text.

Submission of Manuscripts

1. The three copies of the manuscript, including figures and tables, should be sent directly to:
   DR. A. CHOLETTE, editor,
   The Canadian Journal of Chemical Engineering,
   Faculty of Science, Laval University,
   Boulevard de l'Entente,
   Quebec, Que.
2. The authors addresses and titles should be submitted with the manuscript.
3. The author may suggest names of reviewers for his article, but the selection of the reviewers will be the responsibility of the editor. Each paper or article is to be reviewed by two chemical engineers familiar with the topic. Reviewers will remain anonymous.
4. All correspondence regarding reviews should be directed to the editor.

Reprints

1. At least 50 free "tear sheets" of each paper will be supplied.
2. Additional reprints may be purchased at cost. An estimated cost of reprints, with an attached order form, will be sent to the author with the galley proofs.
3. Orders for reprints must be made before the paper has appeared in the Journal.

Communications, Letters and Notes to the Editor

Short papers, as described below, will be considered for publication in this Journal. Their total length should not exceed 600 words, or its equivalent.

Communications

A communication is a prompt preliminary report of observations made which are judged to be sufficiently important to warrant expedited publication. It usually calls for a more expanded paper in which the original matter is republished with more details.

Letters

A letter consists of comments or remarks submitted by readers or authors in connection with previously published material. It may deal with various forms of discussion arising out of a publication or it may simply report and correct inadvertent errors.

Notes

A note is a short paper which describes a piece of work not sufficiently important or complete to make it worth a full article. It may refer to a study or piece of research which, while it is not finished and may not be finished, offers interesting aspects or facts. As in the case of an article a note is a final publication.

* * *

Editorial

WITH this issue, on page 89, *The Canadian Journal of Chemical Engineering* introduces an Industrial Section, devoted to articles of particular interest to the numerous practicing chemical engineers in industry.

To achieve its purpose of promoting the advancement of Chemical Engineering, the Journal has chosen, from the beginning, to publish papers on a variety of subjects. These usually come under one of the following three wide categories.

1. *Original Research*

Original and fundamental research, the starting point of much of the advancement in chemical engineering, can be made most effective and stimulating only through its diffusion in Journals such as this one. Every encouragement will continue to be given to all worthy contributions in the field, whether they promote interest directly or indirectly.

2. *Review Papers*

Much can be gained from a carefully prepared review of existing literature on a given subject, especially when it is critical in nature and aimed at evaluating the relative importance and worth of the papers under consideration. Even if the review material is limited in scope, a review can be effective when incorporated into a comprehensive paper, as long as it constitutes a recognized contribution.

3. *Industrial Papers*

Papers which will henceforth be presented in this new section should represent a wide variety of topics. It is desirable, in general, that they be quantitative rather than qualitative. They can be of particular interest when they bring out some original features in existing or new plants or processes. Special characteristics involving Canadian conditions or the description of Canadian developments could well be the object of a number of stimulating papers.

Without limiting the scope of topics, the subject matter may be expected to deal with such widespread subjects as recent developments in unit operations, flow sheets, applied chemistry, waste treatment and pollution problems, equipment experiences, instrumentation, economics, operations research, etc.

The underlying factor of such papers — which should also constitute the main criterion for their suitability—should be the interest a given paper is likely to arouse in a number of chemical engineers, especially those in industrial practice.

Although the Journal has carried, in the past, a number of papers of interest to industrial people, this number has been somewhat below expectation. The purpose of devoting a special section to industrial papers is to bring more attention to them and thereby foster greater interest and more contributions.

In order to expand this new Industrial Section into a successful and interesting feature — which many readers will look forward to in every issue— the goodwill and benevolent co-operation of a number of readers of the Journal are required. Indeed, the articles that so many would like to read have to come largely from some of the readers themselves.

A great wealth of potentially good material for publication is available to many of our readers who would, one might think, be glad to become authors if only they were encouraged to do so. It is surprising how the slightest encouragement, coming from higher up, can have the effect of an energy of activation and initiate fruitful reactions. The end results may go far beyond what might appear as the mere write-up of something familiar to the writer and his close associates for the benefit of others. Side reactions are often present which turn out to be far more rewarding to everyone than the effort, however important, originally put into the preparation of a paper.

Even though the available subject matter may often be insufficent to warrant full papers, this should be no deterrent to the publication as the Journal now accepts Notes and Communications to the Editor. The terms of references of these sections are outlined in the Instructions to Authors. ★

Effect of Natural Convection on Transition to Turbulence in Vertical Pipes[1]

GEORGE F. SCHEELE[2], EDWARD M. ROSEN[3] and THOMAS J. HANRATTY[2]

The effect of natural convection on transition to a disturbed flow in a heat transfer section of a vertical pipe has been investigated. The transition is related to the distortions of the velocity profile caused by natural convection. When natural convection is in the direction of forced flow the transition appears to occur through the growth of small disturbances. Transition occurs suddenly when natural convection is opposite the direction of forced flow and it appears to be associated with a separation of the flow at the wall.

If a fluid flowing laminarly through a pipe enters a section which is being heated or cooled the velocity distribution will change from a parabola as a result of the variation of the viscosity and the density with temperature over the cross section of the pipe. If the distortions in the velocity profile are large enough transition to an eddying flow can occur. The types of distortions which can be obtained have been discussed in the literature[1,2,3,4,5]. The transition to an eddying flow has been detected from wall temperature measurements[2,6] and from flow patterns of dye that has been injected into the fluid[3,5,7].

The work described in this paper has been done to gain some insight into the mechanism of this transition to a disturbed flow and to relate the stability of the flow to the magnitude of the distortion of the velocity profile. The study has been limited to flows in vertical pipes of circular cross section in which the flow field is being affected by density variation but not significantly by viscosity variation.

Two types of heat transfer experiments have been conducted, one using a constant heat flux at the wall and the other using a constant temperature wall. For the case of a constant heat flux at the wall, if the changes in temperature are affecting only the density appearing in the gravity term a condition is attained far downstream in the heat transfer section such that there is no further change in the velocity profile and such that the temperature and pressure are varying linearly with distance downstream. The maximum distortion of the velocity profile for a completely laminar flow occurs in this region of fully developed flow. For flow through a pipe with a constant wall temperature heat transfer section, the fluid enters at a uniform temperature; if the heat transfer section is long enough the fluid leaves at a uniform temperature equal to the wall temperature. The maximum distortion of the velocity profile occurs at some intermediate position in the heat transfer section.

An exact solution of the Navier-Stokes equations, the continuity equation, and the heat balance equation for the fully developed flow field attained under constant heat flux conditions has been presented by Hallman[2] and by Hanratty, Rosen and Kabel[3]. An approximate solution for the velocity field for heat transfer with a constant temperature wall has been obtained by Rosen[5]. These solutions enable one to compare the stability of a flow field with the maximum distortion of the velocity profile.

The flow stability was examined by injecting a filament of dye into a flowing water stream. The experimental conditions were such that the ratio of the fluid viscosity at the wall and at the pipe center did not exceed about 1.2 and did not go under about 0.8. For these conditions the velocity field obtained for heating in upflow would be the same as for cooling in downflow. These flows are characterized by the fact that natural convection is in the direction of forced flow. Cooling in upflow or heating in downflow involve situations in which natural convection is opposite the direction of forced flow. Constant heat flux experiments were conducted in a pipe wrapped with an electrical heating element under upflow and downflow conditions. Constant temperature wall studies were conducted under upflow conditions in a glass tube possessing a concentric jacket through which the heating or the cooling fluid was circulated at a high rate.

Fully Developed Velocity Profiles for Constant Flux Heat Transfer

For the constant flux heat transfer experiments reported in this paper the fully developed laminar flow velocity profiles are unique functions of Gr/Re_a. Several of these profiles, shown in Figures 1 and 2, have been calculated from the equations presented by Hanratty, Rosen and Kabel[3]. Figure 1 shows velocity fields for cases in which the natural convection is in the direction of flow. For a given flow rate the Gr/Re_a increases with the rate of heat transfer. With increasing Gr/Re_a the velocity profiles flatten out until $Gr/Re_a = 22.0$. At larger Gr/Re_a the profiles have a dimple at their center and the location of the maximum velocity moves toward the pipe wall. The profile attained at $Gr/Re_a = 22.0$ will be referred to as the flat profile in this paper. For $Gr/Re_a > 121.6$ there is a reversal of flow at the center of the pipe. Figure 2 shows velocity profiles for the cases in which natural convection is opposite the direction of flow. In these cases the velocities near the wall are decreased with respect to the isothermal flow field while the velocities in

[1]*Manuscript received December 5, 1959; accepted February 29, 1960.*
[2]*University of Illinois, Urbana, Ill.*
[3]*Applied Mathematics Section, Monsanto Chemical Company, St. Louis, Mo.*
Contribution from the University of Illinois, Urbana, Ill. Based on a paper presented to the C.I.C. Chemical Engineering Conference, Hamilton, Ont., November 9-11, 1959.

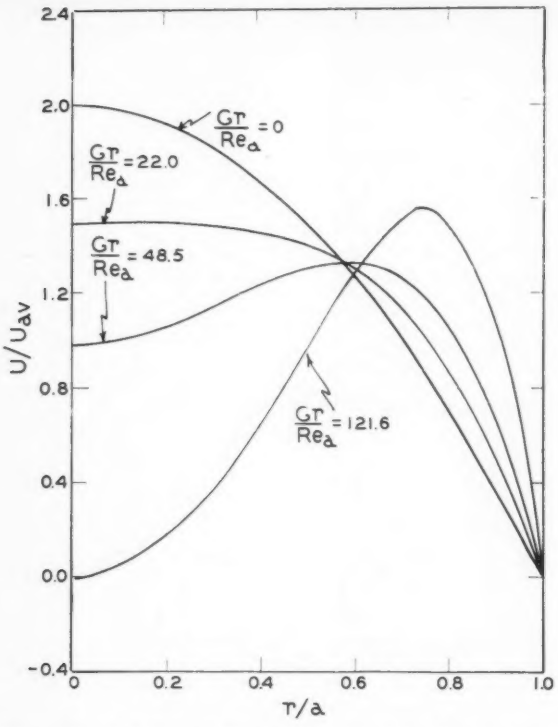

Figure 1—Velocity profiles for heating in upflow-constant wall heat flux.

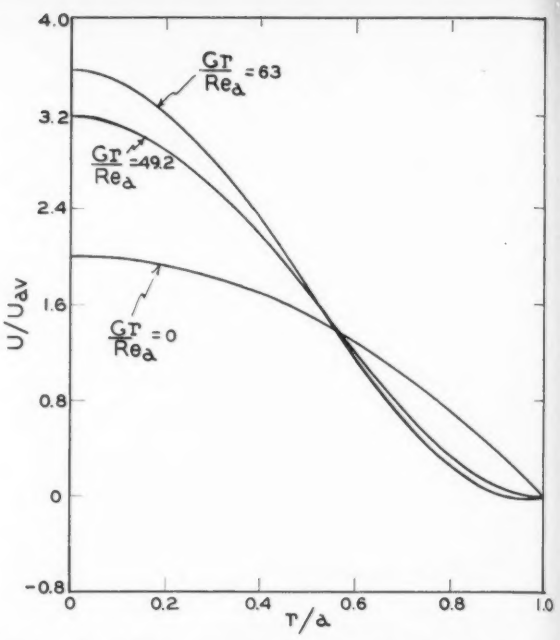

Figure 2—Velocity profiles for heating in downflow with constant wall heat flux.

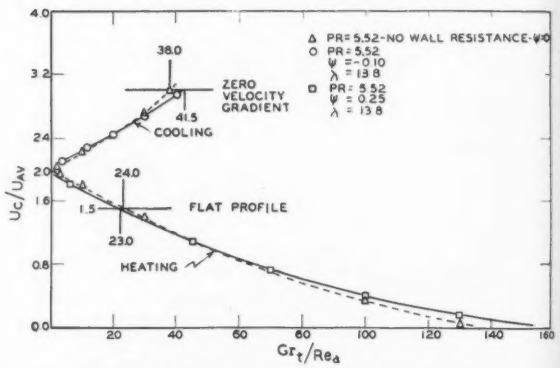

Figure 3—Minimum and maximum center-line velocity for constant temperature heating and cooling in upflow.

the center of the pipe are increased. For $Gr/Re_a = 49.2$ the velocity gradient at the wall is zero and a further increase in Gr/Re_a causes a reversed flow near the wall.

Velocity Profiles for Heat Transfer with a Constant Temperature Wall

Velocity profiles for heat transfer with a constant temperature wall have been calculated by Rosen[5] using an approximate numerical method. The differential equations describing the velocity profile and the temperature profile were simplified by making use of the boundary layer assumptions. Equations were assumed to represent the velocity and temperature profiles in which there were a number of coefficients which were functions of the distance downstream. For example, the velocity profile was represented by the equation

$$\frac{U}{U_{AV}} = k_1 + k_2\left(\frac{r}{a}\right)^2 + k_3\left(\frac{r}{a}\right)^4$$

The variation of the coefficients, k_1, k_2, k_3, was defined by means of integral relationships such as a mass balance and a mechanical energy balance, by boundary conditions, such as the velocity being zero at the wall, and by conditions derived from the differential equations, such as the equation of motion at the center of the pipe. Both the density and the viscosity were allowed to vary and account was taken of the finite resistance of the wall to heat transfer such that the temperature of the inside wall was varying although the temperature of the outside wall was kept constant. The velocity field is found to be a function of the Graetz number, Gz, the ratio of the Grashof and Reynolds numbers, Gr_t/Re_a, the Prandtl number, Pr, a parameter ψ related to the ratio of the viscosity at the wall to the viscosity at the entrance, and a wall resistance parameter, λ. This solution has been used to calculate the changes in the velocity. For the experiments described in the paper the values of Pr and λ were approximately constant and the effect of ψ was small enough that it could be represented by an average value. In Figure 3 the calculated minimum or maximum centerline velocity is plotted as a function of Gr_t/Re_a for heating and cooling in upflow for conditions corresponding to the experiments. For heating in upflow a flat profile corresponding to the profile at $Gr/Re_a = 22.0$ for the fully developed constant heat flux condition occurs for $U_c/U_{AV} = 1.5$ for the approximate velocity profile which has been used. For cooling the condition of zero velocity gradient at the wall occurs for $U_c/U_{AV} = 3.0$ for the approximate profile used. The calculated locations of the flat velocity profile and the minimum velocity profile are plotted in Figure 4 as a function of Gr_t/Re_a for heating in upflow. In Figure 5 the calculated location of the zero velocity gradient at the wall is plotted as a function of Gr_t/Re_a for cooling in upflow. For comparison calculated velocities and locations for zero wall resistance, $\lambda = \infty$, and constant viscosity, $\psi = 0$, are presented in Figures 3, 4 and 5. It should be noted that the difference between the two sets of curves is due to changes in both the wall resistance parameter, λ, and the viscosity ratio parameter, ψ

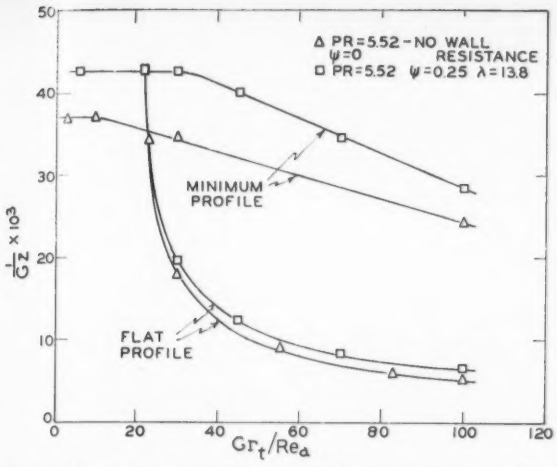

Figure 4—Location of flat and minimum velocity profiles for constant temperature heating in upflow.

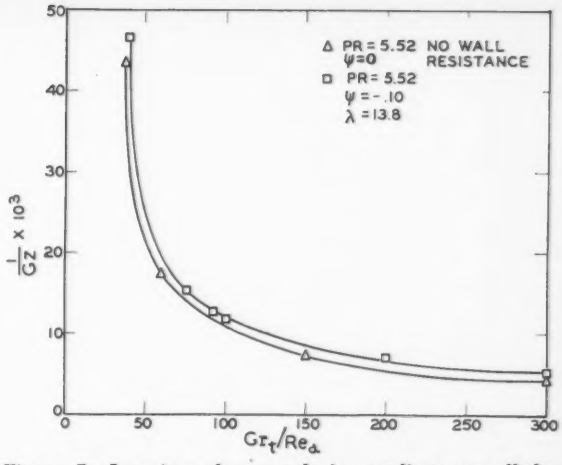

Figure 5—Location of zero velocity gradient at wall for constant temperature cooling in upflow.

Equipment Design

Transition to an unstable flow was detected by observing the breakup of a thin stream of dye injected into the center of the tube upstream of the heat transfer section. Additional observations were made by flooding the flow field with dye and then purging this dye.

For constant heat flux experiments the heat transfer section was a 71½ in. vertical length of ⅝ in. I.D. brass tube (L/D = 114.3). The tube was wrapped with a layer of thermosetting electrical tape to insulate it electrically from the heating element which was Chromel-A heating wire ⅛ in. × 0.004 in. wrapped uniformly about the tube. Current was supplied to the heating element from a 115 volt AC line, and the input to the heater was measured with a calibrated wattmeter.

Surrounding the heat transfer section was a vacuum jacket constructed of 1½ in. I.D. Plexiglas tubing fitted concentrically to the brass tube to reduce convection heat losses. A pressure of 5 mm. Hg or lower was used in the jacket. A layer of aluminum foil was placed over the inside surface of the jacket to reduce radiation heat losses.

Calming sections of ⅝ in. I.D. Plexiglas tubing 72 in. in length (L/D = 115) were placed at both ends of the heat transfer section to dampen out disturbances in the flow caused by the entry so that the flow would achieve a fully-developed parabolic velocity profile before entering the heat transfer section. Plexiglas was used so that the motion of the dye leaving the heat transfer section could be observed visually.

Room temperature water was supplied from a 54 gallon constant head tank to either the top or the bottom of the apparatus depending on whether downflow or upflow experiments were to be run. Approximate flow rates were set with a rotameter, but the actual flow rates were determined by collecting and weighing the water.

Methylene blue dye was injected into the system through a No. 18 hypodermic needle attached to the end of a ⅛ in. O.D. brass tube that was centered by triangular spacers 2, 6, 15, and 24 in. from the probe tip. The probe tip was located 38 in. upstream from the entry to the heat transfer section. Reynolds numbers of 450 (based on radius) could be obtained before disturbances due to the probe affected the dye stream.

For constant temperature experiments the test section was a 306 cm. vertical length of Pyrex brand chemical glass with I.D. = 2.19 cm. and O.D. = 2.50 cm. Surrounding the glass tube was a 3.80 cm. I.D. plastic jacket divided into an upper and a lower section. For heating in upflow room temperature water passed through the inner tube and the lower jacket while hot water was pumped through the upper jacket at a high rate. For cooling in upflow hot water passed through the inner tube and the lower jacket while room temperature water was pumped at a high rate through the upper jacket. The lower constant temperature section, which served as a calming section so that a parabolic profile would develop, was 123.2 cm. long (L/D = 56.3) and the heat transfer section was 182.5 cm. long (L/D = 83.3).

Water was supplied to the test section from a constant head tank. Approximate flow rates were set with a rotameter, but to determine the actual flow rate the water was weighed. Methylene blue dye was introduced through a ⅛ in. I.D. brass tube fitted with a No. 20 hypodermic needle at its tip. The tip was 50 cm. upstream from the start of the heat transfer section and the spacers used to locate the injector in the tube center were 8 cm. and 30 cm. from the tip.

Thermocouples for measuring temperature were located at the inlet and outlet of the test sections and at the inlet and outlet to each jacket.

Procedure

During an experimental run the flow rate was the variable adjusted until the transition point was obtained. Transition was defined as that condition when the dye filament first deviated from its streamline motion and became slightly sinuous or burst into turbulence.

In the constant flux case the motion of the dye stream could be observed only at the outlet from the heated section and, therefore, at a fixed L/D of 114.3. For constant temperature heating or cooling the flow field could be viewed over the entire length of the heat transfer section except for the last 12 cm. where the overflow system obscured observations. This gave an effective visible length of 170 cm. (L/D = 77.6).

Values of Re_a less than 40 could not be studied because the low water flow rate caused the dye filament to become too diffuse downstream. Values of Re_a greater than 350 were not studied because of the possible effect of disturbances due to the dye injector on the dye stream at these relatively large flow rates. However, experiments in which dye was purged from the field could be carried out at larger flow rates.

It was not possible to determine the transition point exactly for a given Grashof number because of the difficulty in visually detecting the first slight disturbance of the dye filament. Since the flow became unstable as the flow rate was decreased, the transition Reynolds number was calculated from the arithmetic average of the lowest flow rate for which no disturbance of the dye filament was observed and the highest flow rate for which a disturbance was detected. A similar averaging process was used to determine the asymmetry point for experiments with a constant temperature wall. This average flow rate was within

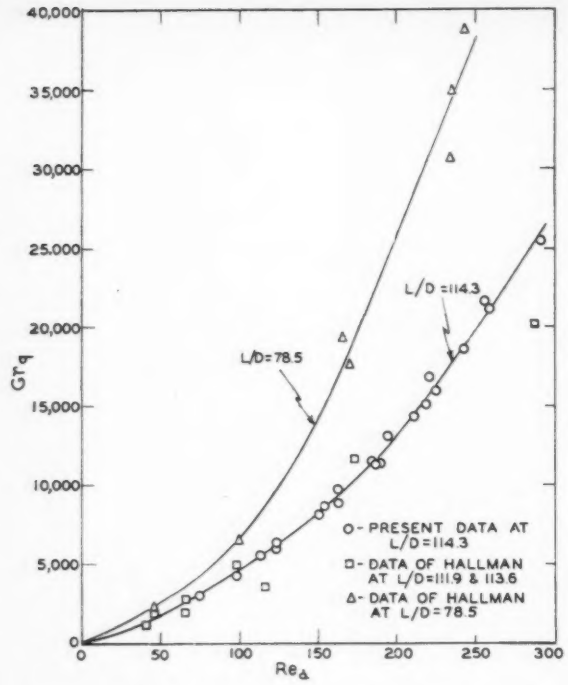

Figure 6—Upflow transition for constant flux heating.

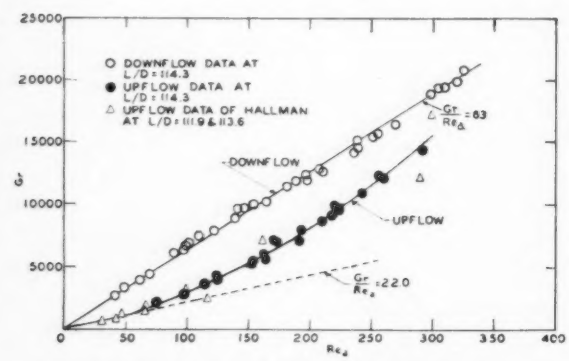

Figure 7—Transition for constant flux heating.

1% of the two flow rates from which it was calculated for constant flux heat transfer and within 5% for heat transfer runs using a constant temperature wall.

It was necessary to correct for heat losses in the constant heat flux experiments in order to calculate the heat input to the water from measurement of the electrical energy produced by the heating element. Radial heat losses were determined by isolating the heat transfer section from the rest of the system, filling it with water, applying a constant heat input to the heater, and measuring the electrical energy dissipation as a function of the difference between the steady-state average water temperature and the atmospheric temperature.

Some bulk temperature measurements were made at the entrance and exit from the heat transfer section, and the heat input obtained from these measurements was compared with the wattage corrected by radial heat loss data. There was an average deviation of 1.3% in the determination of heat input. The close agreement of the two methods justified the use of radial heat losses to calculate the heat input to the water.

For the constant temperature wall case all fluid properties were evaluated at the inlet temperature. Fluid properties for the constant heat flux case were also evaluated at inlet conditions because the location of the onset of turbulence could not be determined in the experiments and because the bulk temperature rise in the heat transfer section was less than 6°F. in all runs. In calculating Hallman's data for comparison purposes fluid properties were also evaluated at the inlet temperature, although Hallman used an arithmetic average of the bulk temperature and the wall temperature at the transition point in presenting his data.

For constant heat flux experiments heat input and flow rate were the two variables examined. The data for this case are presented in terms of a Grashof number, Gr_q, based on heat input to the water and a Reynolds number, Re_a, based on radius. This modified Grashof number is defined as the product of the Grashof number, Gr, based on the difference between the wall and center-line fluid temperatures and the modified Nusselt group used by Hanratty, Rosen and Kabel. It has the following dimensionless form

$$Gr_q = \frac{a^4 \rho_a^2 g \beta_a q}{k_a \mu_a^2}.$$

The data are also presented in terms of Gr. The temperature differences used in these values of Gr were computed from experimental values of heat input by using the modified Nusselt group plots of Hanratty, Rosen and Kabel which relate heat flux to temperature difference $T_w - T_c$ for fully-developed flow conditions. For constant wall temperature experiments the data are presented in terms of a Grashof number, Gr_t, based on the temperature difference between the heating or cooling jacket water and the inlet water and a Reynolds number, Re_a.

Results with Constant Flux Heat Transfer

When the flow was isothermal the dye emerged from the heat transfer section as a filament in the center of the pipe. For constant flux heating in upflow (natural convection in the direction of flow) the first instability was noted as sinuous motion in the emerging dye filament. Further decrease in the Reynolds number, keeping the Grashof number constant, caused an increase in the amplitude of the disturbances and eventually breakup of the dye filament.

In Figure 6 the Grashof number Gr_q required for transition is plotted as a function of Re_a. Included on the graph are experimental data of Hallman[2] obtained at L/D of 113.6, 111.9, and 78.9 for comparison with present experimental data at L/D = 114.3. The scatter in Hallman's data as plotted in Figure 6 may be due to a viscosity effect caused by the large temperature differences in his experiments. Fully developed laminar flow velocity profiles are unique functions of Gr/Re_a only if the variation of viscosity with temperature is neglected. The agreement with present data at the same L/D value can be seen on the graph. Hallman's data indicate an effect of L/D on transition as can be seen by comparing the curve at L/D = 78.5 with the one at L/D = 114.3. The longer pipe requires a smaller input of heat to cause transition for a given flow rate. In Figure 7 the Grashof number Gr, based on the difference between the wall and center-line fluid temperatures, is plotted as a function of Re_a at transition. The critical value of Gr/Re_a increases from 22 to 50 as Re_a increases from 50 to 290. For comparison a straight line representing Gr/Re_a = 22.0, the value at which the velocity profile becomes flat, is also shown in Figure 7.

For constant flux heating in downflow (natural convection opposite the direction of flow) the first instability consisted of a slight asymmetry of the dye filament emerging from the heat transfer section. This was followed by intermittent bursts into a highly disturbed flow. Further decrease in the flow rate, keeping the heat flux constant, increased the frequency of appearance of these bursts.

Figure 8 is a plot of Gr_q versus Re_a for the first appearance of these bursts and in Figure 7 is a plot of the Grashof number,

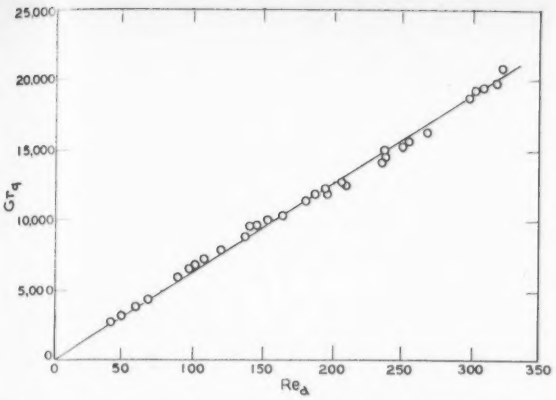

Figure 8—Downflow transition at $L/D = 114.3$ for constant flux heating.

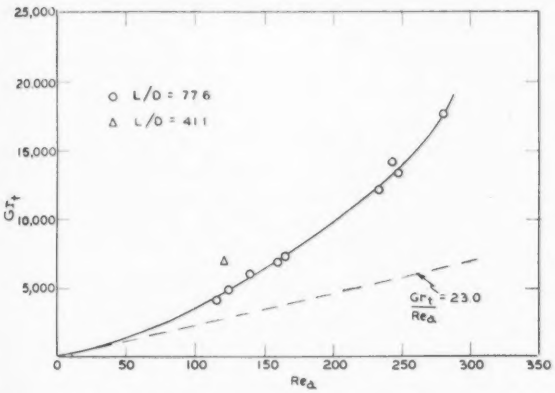

Figure 10—Transition for upflow heating-constant wall temperature case.

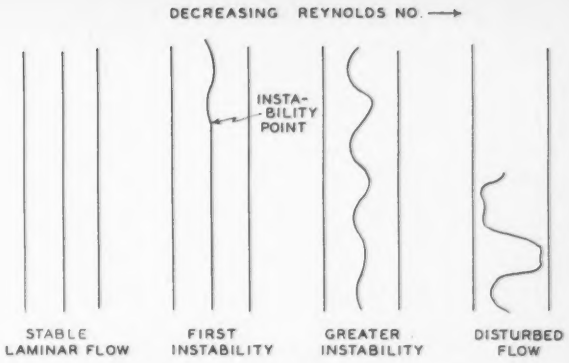

Figure 9—Transition process for heating in upflow viewed at fixed L/D for constant Grashof number.

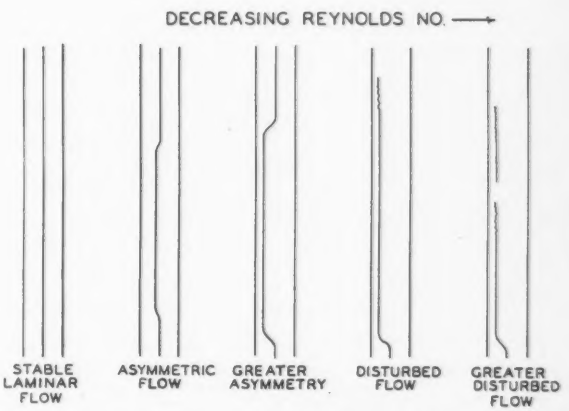

Figure 11—Transition process for cooling in upflow at constant Grashof number; dye filament behavior.

Gr, based on the difference between the wall and center-line fluid temperatures, versus Re_a. The critical value of Gr/Re_a is 63 and is constant over the range of Re_a studied. Tabulated data for Figures 6, 7, and 8 are presented by Scheele[7].

Results for Heat Transfer with a Constant Temperature Wall

For constant temperature wall experiments it was possible to observe the entire heat transfer section rather than just the outlet as in constant heat flux experiments. As in the case of constant flux heat transfer the first instability for a constant temperature wall when the natural convection was in the direction of flow was a sinuous motion of the dye filament. This instability was located just at the outlet of the heat transfer section indicating that the data were influenced by the L/D ratio. A decrease in the flow rate, keeping the temperature difference constant, caused the point at which sinuous motion was first observed to move upstream. The amplitude of the sinuous motion increased with downstream distance. At low enough flow rates the amplitude of the sinuous motion became so large that the dye filament broke up and appeared to be completely mixed with the water. Sketches of the flow patterns observed with the dye filament are shown in Figure 9.

In Figure 10 the Grashof number Gr_t, based on the difference between the jacket and inlet water temperatures, is plotted as a function of Re_a at transition for heating in upflow with a constant temperature wall. There is one point at $L/D = 41.1$ to compare with the transition data for $L/D = 77.6$. An effect of L/D similar to that observed for constant flux heat transfer was observed. A straight line representing $Gr_t/Re_a = 23.0$, the value at which a flat velocity profile is first obtained, is also shown. The location of the instability point is compared with the calculated locations of the flat velocity profile and the minimum velocity profile in Table I. The location of the initial instability was always observed downstream of the location of the flat profile.

For heat transfer with a constant temperature wall in which natural convection opposed the flow the first flow instability noted was a shift of the dye stream from the center of the pipe. Far enough downstream the dye stream returned to the pipe center. As the flow rate was decreased, keeping the temperature difference constant, the asymmetry of the dye stream increased. Eventually breakup of the dye filament was noted. The breakup point varied with time and with position in an apparently random fashion. In the interval between breakups the dye stream was undisturbed. At low Re_a there was a range of flow rates between the initial appearance of the asymmetry and the first breakup of the dye filament. At higher Re_a breakup occurred as soon as the flow field became slightly asymmetric. Sketches of the observed transition process are shown in Figure 11. Additional information on the asymmetries was obtained by flooding the flow field with dye and then purging the dye from the field. At a given temperature difference and a large flow rate the dye flooded the entire field, and purging cleared the dye from the heat transfer section. At lower Reynolds numbers a portion of the flow field near the wall on one side of the pipe in the heat transfer section remained clear when the pipe was flooded with dye. When the dye was purged the formerly clear region remained colored long after the rest of the flow field became clear. Within this region it was observed that

TABLE 1

CONSTANT TEMPERATURE HEATING IN UPFLOW: COMPARISON OF LOCATION OF INSTABILITY WITH VELOCITY PROFILE DISTORTIONS

FOR $\lambda = 13.8$, $\psi = 0.25$

Run	Re_a	Experimental Location of Instability		Calculated Location of Flat Profile		Calculated Location of Minimum Center Velocity	
		(Z/D)	Gz	(Z/D)	Gz	(Z/D)	Gz
1	280	77.6	29.8	21.5	108	83.9	27.5
2	248	77.6	26.1	21.2	95.2	77.0	26.2
3	116	77.6	15.2	19.2	61.3	49.4	23.9
4	166	77.6	21.4	21.4	77.5	67.1	24.8
5	234	77.6	28.9	24.5	91.7	86.5	26.0
6	243	77.6	29.7	22.8	101	85.6	26.9
7	142	77.6	16.0	16.5	75.2	50.5	24.6
8	125	77.6	13.7	15.3	69.4	43.7	24.3
9	160	77.6	17.4	17.8	75.8	54.7	24.7
10	140	59.4	19.5	13.9	83.3	45.9	25.3
11	122	41.1	24.4	10.0	100	37.6	26.7

there was a downflow. A further decrease in flow rate caused a wider region of downflow on one side of the pipe which became unstable downstream. The circumferential position of this asymmetric region of reverse flow varied from run to run in apparently random fashion. The point in the pipe at which asymmetry was first observed moved downstream as the flow rate at which asymmetry first appeared increased, as can be seen in Table 2. Sketches of the flow patterns observed in these purging experiments are shown in Figure 12.

Curves representing the conditions at which asymmetry was first observed and the conditions at which instability of the dye filament first occurred are plotted in Figure 13. The conditions under which the flow became asymmetric were determined both by observing the motion of a dye stream and by flooding the field with dye, and these two methods gave the same result. Asymmetric flow first occurs for $Gr_t/Re_a = 74$ and this value is constant over the range of Re_a studied. The conditions under which transition to an eddying flow occured could not be determined satisfactorily using the flooding technique, and so these instability data were obtained only from observations of the motion of a dye filament. The value of Gr_t/Re_a for transition

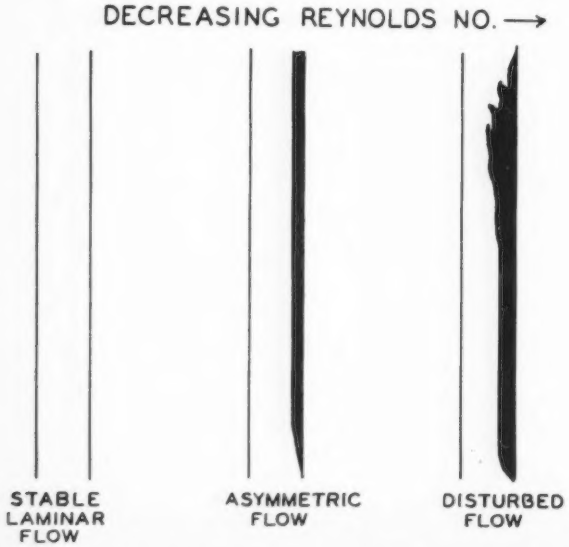

Figure 12—Transition process for cooling in upflow at constant Grashof number; purged dye field behavior.

TABLE 2

CONSTANT TEMPERATURE COOLING IN UPFLOW: COMPARISON OF LOCATION OF INSTABILITY AND OF ASYMMETRY WITH VELOCITY PROFILE DISTORTION

FOR $\lambda = 13.8$, $\psi = -0.10$

Run	Re_a	Experimental Location of Instability		Experimental Location of Asymmetry		Calculated Location of Zero Velocity Gradient at the Wall	
		(Z/D)	Gz	(Z/D)	Gz	(Z/D)	Gz
2	248	73.1	30.0			28.4	77
3	232	70.8	28.3			24.3	82
5	47.2	near entry				3.4	133
6	114	4.6	229			8.4	125
7	240	59.4	37.5			27.5	81
8	88.4	9.1	88.7			6.9	117
9	91.0	9.1	89.1			7.4	110
10	142			4.6	283	16.7	78
11	231			11.4	181	27.2	76
12	192			9.1	195	23.6	75
13	120			6.8	166	15.7	72
14	296			11.4	225	32.8	78
15	346			11.4	263	37.4	80
16	654			22.8	233	71.7	74

to an eddying flow varies from 141 to 75 as Re_a increases from 50 to 250. The determination of the asymmetry point could be made at higher Reynolds numbers than the other transitions studied since the purging did not introduce disturbances into the flow as did the probes used to introduce the dye filament. In Table 2 the locations of the instability and asymmetry points are compared with the calculated position in the pipe at which the velocity gradient at the wall is zero. Asymmetry generally occurred upstream of the location at which the wall velocity gradient is zero, but instability occurred downstream of this location. Since the theory is least satisfactory in the region close to the entry, it may be that asymmetry always occurred downstream of the point at which the wall velocity gradient actually becomes zero. It should be pointed out that the calculations were made for a symmetric flow field while the experimental flow fields were asymmetric.

DISCUSSION

Natural Convection in the Direction of Flow

For heat transfer in which natural convection is in the direction of flow, the experiments reported in this paper show that the velocity profile must be distorted at least to a condition of flatness in order for a transition to sinuous flow to occur. This is supported by the data in Figure 7 which indicate transition in

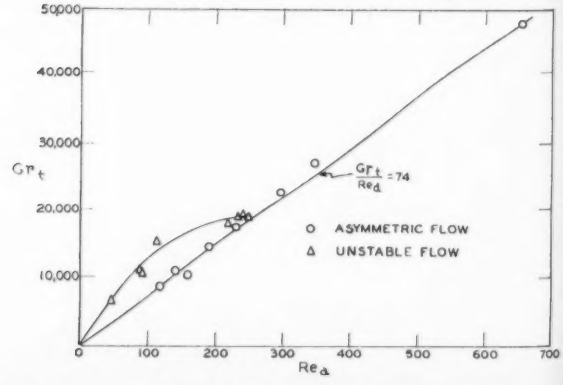

Figure 13—Transition for upflow cooling-constant wall temperature case.

all cases for $Gr/Re_a \geq 22.0$ and by the data in Figure 11 which indicate transition for $Gr_t/Re_a \geq 23.0$. Likewise in Table 1 it is shown that for constant temperature wall runs the initial instability occurred downstream of the location in the pipe at which the velocity profile became flat.

The mechanism of transition to an eddying flow in these cases consists of the appearance of regular oscillations which grow in extent and amplitude until the waves become distorted and break into fluctuations characteristic of turbulent flow. This mechanism is similar to that observed by Schubauer and Skramstad for boundary layer transition in air flowing over a flat plate[8].

Direct experimental observation and the fact that the sinuous disturbances first appeared at the outlet of the heat transfer section indicate that the L/D ratio is affecting transition. This effect can result from the use of a length of pipe insufficient for infinitesimal disturbances in the fluid to grow into disturbances that can be seen. In the constant heat flux experiments it can also result from the use of an insufficient length of pipe to obtain fully developed flow. Experimental correlations developed by Hallman[2] and theoretical results presented by Sellars, Tribus, and Klein[9] indicate that in all the experiments reported in this paper the temperature profile at the exit of the heat transfer section was at least 95% fully developed. In the constant temperature wall case the possibility of an L/D effect would be excluded if the pipe were long enough for the flow to be isothermal at the outlet of the heat transfer section. This was not so for the transition data reported. In all cases the velocity profile at the outlet of the heat transfer section was still quite distorted from the parabolic flow obtained under isothermal conditions.

Natural Convection Opposite the Direction of Flow

In all experiments in which natural convection is opposite the direction of flow, transition to an eddying flow is associated with separation of the flow at the wall. For constant temperature cooling in upflow an asymmetric region of reverse flow occurred for $Gr_t/Re_a = 74$, while theory predicts that reverse flow will occur for all Gr_t/Re_a greater than 41.5. This asymmetry does not appear to be due to asymmetry in the experimental equipment since the same apparatus was used for constant temperature heating in upflow runs where no asymmetry was detected. In Figure 13 it can be seen that while at high Reynolds numbers even slightly asymmetric flow fields are unstable, at lower Reynolds numbers stable asymmetric flows exist. For constant flux heating in downflow breakup of the flow occurred for $Gr/Re_a = 63$, while theory predicts that reverse flow will occur for all Gr/Re_a greater than 49.2.

These data and visual observations indicate that the mechanism of breakup is as follows: A symmetrical downward flow at the wall becomes unstable and an asymmetric condition develops in which there is a downward flow at the wall on one side of the heat transfer section. With increasing Gr_t/Re_a the region of downward flow increases in size until transition to an eddying flow occurs. This occurrence of an asymmetric flow field is in agreement with observations of Hallman[2] who found that his constant heat flux downflow runs were characterized by an asymmetry in wall temperature which became more severe as the heating rate increased.

The transition to an eddying flow did not occur through a gradual growth of small disturbances but by means of a process which occurred suddenly. The transition appeared to be similar to that described for separated boundary layer flows along flat plates[10,11]. That no effect of L/D on the transition data was apparent could be explained by the fact that the transition occurred more suddenly than for heat transfer in which natural convection was in the direction of the flow.

Acknowledgment

The authors gratefully acknowledge financial support from the Consolidation Coal Company and the National Science Foundation in the form of fellowship grants to George F. Scheele.

Nomenclature

a = inside radius of the pipe, ft.
C_p = heat capacity at constant pressure, B.t.u./(lb.) (°F)
d = outside radius of the pipe, ft.
D = inside diameter of the pipe, ft.
g = acceleration of gravity equal to 4.17×10^8 ft./hr.^{2}
Gr = Grashof number based on the difference between the center line temperature and the wall temperature, $\dfrac{a^3 \rho_o^2 g \beta_o |T_w - T_c|}{\mu_o^2}$
Gr_q = Grashof number based on the heat flux, $\dfrac{a^4 \rho_o^2 g \beta_o q}{k_o \mu_o^2}$
Gr_t = Grashof number based on the difference between the entrance temperature and the jacket temperature, $\dfrac{a^3 \rho_o^2 g \beta_o |T_w - T_o|}{\mu_o^2}$
Gz = Graetz number, $\pi Re_a \, Pr \, a/Z$
k, k_s = thermal conductivity of the fluid and wall respectively, B.t.u./ (hr.) (ft.) (°F.)
k_n = coefficients of the velocity profile series
L = total length of heat transfer section, ft.
Pr = Prandtl number, $C_p \mu / k$
q = heat flow at the wall, B.t.u./(hr.) (ft.^{2})
r = radial position, ft.
Re_a = Reynolds number based on the radius, $\dfrac{a U_{AV} \rho_o}{\mu_o}$
T_c = temperature at the center of the pipe, °F.
T_o = temperature at the entrance of the pipe, °F.
T_w = temperature of the fluid in the jacket for constant temperature wall experiments; temperature of the inside wall of the pipe for constant heat flux experiments, °F.
U = local velocity, ft./hr.
U_{AV} = average velocity, ft./hr.
U_c = velocity at the center of the pipe, ft./hr.
Z = distance measured downstream from the start of the heat transfer section, ft.
β = coefficient of cubical expansion, °F.$^{-1}$
λ = wall resistance parameter $k_s/k \, ln \, (d/a)$
μ = viscosity of the fluid, lb./(ft.) (hr.)
ρ = density of the fluid, lb./ft.^{3}
ψ = related to ratio of viscosity at wall to viscosity at entrance, $\dfrac{\mu_w}{\mu_o} = \dfrac{1}{1 + \psi}$
o = subscript for fluid properties evaluated at entrance conditions

References

(1) Apostolakis, N., M.S. Thesis in Chemical Engineering, University of Illinois, Urbana (1957).

(2) Hallman, T. M., Trans. A.S.M.E., **78,** 1831 (1956); Ph.D. Thesis in Mechanical Engineering, Purdue University, Lafayette (1958).

(3) Hanratty, T. J., Rosen, E. M., and Kabel, R. L., Ind. Eng. Chem., **50,** 815 (1958).

(4) Pigford, R. L., Chem. Eng. Prog. Symposium Series, No. 17, Vol. 51; A.I.Ch.E. Annual Meeting, St. Louis (1953).

(5) Rosen, E. M., Ph.D. Thesis in Chemical Engineering, University of Illinois, Urbana (1959).

(6) Guerrieri, S. A., Hanna, R. J., "Local Heat Flux in a Vertical Duct with Free Convection in Opposition to Forced Flow", ONR Final Rept., Contract N-ONR-622 (01) (November, 1952).

(7) Scheele, G. F., M.S. Thesis in Chemical Engineering, University of Illinois, Urbana (1959).

(8) Schubauer, G. B. and Skramstad, H. K., NACA Rept. 909 (1948).

(9) Sellars, J. R., Tribus, M., and Klein, J. S., Trans. A.S.M.E., **78,** 441 (1956).

(10) Lochtenberg, B. H., "Transition in a Separated Laminar Boundary Layer", Aeronautical Research Council, 19,007 F.M. 2495, Great Britain (January, 1957).

(11) Maekawa, T. and Atsumi, S., NACA Tech. Mem. 1352 (1952).

★ ★ ★

Critical Velocity of Gas[1]

A. P. BUTHOD[2] and CHI TIEN[3]

Expression of critical velocity, based on thermodynamic consideration was obtained and is given by the following equation:

$$u_c = \sqrt{\frac{Z\,R\,T_r\,T_c\,g_c}{\left[1 - \frac{\partial\ ln\ Z}{\partial\ ln\ p_r}\right] - \frac{R\,Z\left[1 + \frac{\partial\ ln\ Z}{\partial\ ln\ T_r}\right]^2}{C_p}}}$$

or the ratio between the critical velocity and that of a corresponding ideal gas is given by

$$\frac{u_c}{u_c^{\sharp}} = \frac{1/\gamma^{\sharp}}{X - Y\,\frac{R}{C_p}}$$

where $X = \left[1 - \frac{\partial\ ln\ Z}{\partial\ ln\ p_r}\right]/Z$

$$Y = \left[1 + \frac{\partial\ ln\ Z}{\partial\ ln\ T_r}\right]^2$$

$$\gamma^{\sharp} = C_p^{\sharp}/(C_p^{\sharp} - R)$$

Numerical values of *X* and *Y* were computed and presented on the generalized plot basis. Together with the value of heat capacity, this method enables the rapid calculation of critical velocity of real gas when the deviation from ideal gas behavior is significant.

In the study of compressible fluid flow, the ideal gas behavior is often assumed. This assumption has been quite satisfactory for low pressures. But as the deviation from ideal behavior becomes pronounced with the increase of pressure, the validity of ideal behavior no longer exists. This is true in the case of critical velocity as demonstrated in earlier experimental work[1,2].

Several suggestions have been proposed to remedy this situation. One of the common approaches, for example, as in the study of isentropic flow of steam, involves the use of enthalpy-entropy diagram. This method is quite tedious and moreover, with the exception of very few common compounds, this type of thermodynamic information is not available. Some analytical work along this line has been reported in literature. Tsien[3] studied the one-dimensional flow problem of gases characterized by van der Waals' equation and gave both analytical expressions and numerical results. A later work by Crown[4] treated the case with the equation of state given by the Beattie-Bridgeman equation. Tsien's results are very elegant and fairly simple to use but unfortunately the van der Waals' equation does not truly describe the behavior of real gas especially in the neighbourhood of critical region. The Beattie-Bridgeman equation, on the other hand, gives a very good agreement with the actual gas behavior but since the original equation consists of so many terms, the resulting expression becomes too involved for rapid calculation.

The purpose of this work is to present a general method which enables the calculation of critical velocity of any real gas with ease and accuracy. This is made possible through the advances in the field of generalized thermodynamic properties accomplished in recent years.

Theoretical Consideration

The critical velocity, or sound velocity, through a fluid is given by the following expression:

$$u_c^2 = g_c\left(\frac{\partial P}{\partial \rho}\right)_s \qquad (1)$$

Since the density is the reciprocal of specific volume, Equation (1) can be rewritten as

$$u_c^2 = -\,v^2\left(\frac{\partial P}{\partial v}\right)_s g_c \qquad (2)$$

From the thermodynamic consideration, it can be shown that

$$\left(\frac{\partial p}{\partial v}\right)_s = -\,\frac{C_p}{C_v}\left(\frac{\partial P}{\partial T}\right)_v \Big/ \left(\frac{\partial v}{\partial T}\right)_p \qquad (3)$$

Using the general expression, $Pv = ZRT$, as equation of state, the two partial derivatives on the right side of Equation (3) can be expressed as

$$\left(\frac{\partial v}{\partial T}\right)_p = \frac{ZR}{p} + \frac{RT}{p}\left(\frac{\partial Z}{\partial T}\right)_p \qquad (4)$$

and

$$\left(\frac{\partial P}{\partial T}\right)_v = \frac{ZR}{v} + \frac{RT}{v}\left(\frac{\partial Z}{\partial T}\right)_v \qquad (5)$$

Consider Z as a function of temperature and pressure, the partial derivative, $\left(\frac{\partial Z}{\partial T}\right)_s$ can be expressed as

$$\left(\frac{\partial Z}{\partial T}\right)_s = \left(\frac{\partial Z}{\partial T}\right)_p + \left(\frac{\partial Z}{\partial p}\right)_T \left(\frac{\partial P}{\partial T}\right)_s \qquad (6)$$

[1]*Manuscript received September 23, 1959; accepted February 19, 1960.*
[2]*The University of Tulsa, Tulsa, Oklahoma.*
[3]*Essex College, Assumption University of Windsor, Windsor, Ont.*
Contribution from The University of Tulsa, Tulsa, Oklahoma.

Substituting Equation (6) into Equation (5) and after rearrangment, we have:

$$\left(\frac{\partial P}{\partial T}\right)_v = \frac{ZR + RT\left(\frac{\partial Z}{\partial T}\right)_p}{v - RT\left(\frac{\partial Z}{\partial p}\right)_T} \quad \ldots\ldots(7)$$

Another thermodynamic relationship between heat capacities at constant pressure and at constant volume is:

$$C_p - C_v = T\left(\frac{\partial P}{\partial T}\right)_v \left(\frac{\partial v}{\partial T}\right)_p \quad \ldots\ldots(8)$$

Rearranging Equation (8), we obtain the expression for the ratio of these two heat capacities:

$$\frac{C_p}{C_v} = \frac{1}{1 - \left(\frac{T}{C_p}\right)\left(\frac{\partial P}{\partial T}\right)_v \left(\frac{\partial v}{\partial T}\right)_p} \quad \ldots\ldots(9)$$

Substituting Equation (9) into Equation (3) we have:

$$\left(\frac{\partial P}{\partial v}\right)_s = \frac{-\left(\frac{\partial P}{\partial T}\right)_v}{\left(\frac{\partial v}{\partial T}\right)_p - \frac{T}{C_p}\left(\frac{\partial P}{\partial T}\right)_v \left(\frac{\partial v}{\partial T}\right)_p^2} \quad \ldots\ldots(10)$$

By further substitution Equations (4) and (7) into Equation (10), the following expression results:

$$\left(\frac{\partial P}{\partial v}\right)_s = \frac{-1}{\frac{RTZ}{p^2}\left[1 - \frac{\partial\ ln\ Z}{\partial\ ln\ p_r}\right] - \frac{T\,R^2\,Z^2}{C_p\,p^2}\left[1 + \frac{\partial\ ln\ Z}{\partial\ ln\ T_r}\right]^2} \quad (11)$$

The expression for critical velocity becomes

$$u_c^2 = -v^2\left(\frac{\partial p}{\partial v}\right)_s g_c,$$

$$= \frac{Z\,R\,T_r\,T_c\,g_c}{\left[1 - \frac{\partial\ ln\ Z}{\partial\ ln\ p_r}\right] - RZ\frac{\left[1 + \frac{\partial\ ln\ Z}{\partial\ ln\ T_r}\right]^2}{C_p^\phi + [C_p - C_p^\phi]}} \quad \ldots\ldots(12)$$

For ideal gases, $Z = 1$, $\frac{\partial\ ln\ Z}{\partial\ ln\ T_r} = 0$, $\frac{\partial\ ln\ Z}{\partial\ ln\ p} = 0$, $C_p - C_p^\phi = 0$

and $C_p^\phi - R = C_v^\phi$, equation (12) reduces to the familiar form as:

$$u_c^\phi = \sqrt{R\ T_r\ T_c\ \gamma^\phi\ g_c}, \quad \ldots\ldots(13)$$

$$\text{where } \gamma^\phi = \frac{C_p^\phi}{C_v^\phi} = \frac{C_p^\phi}{C_p^\phi - R}$$

Sometimes, it is more convenient to express a quantity in terms of the ratio of this quantity to that of an ideal model. For critical velocity of real gas, this can be done by comparing the actual value with that of an ideal gas with the same critical properties. This gives,

$$\frac{u_c}{u_c^\phi} = \sqrt{\frac{(1/\gamma^\phi)}{X - \frac{RY}{C_p^\phi + (C_p - C_p^\phi)}}} = \sqrt{\frac{(1/\gamma^\phi)}{X - \frac{RY}{C_p}}} \quad \ldots(14)$$

where

$$X = \left(1 - \frac{\partial\ ln\ Z}{\partial\ ln\ T_r}\right) \Big/ Z$$

$$Y = \left[1 + \frac{\partial\ ln\ Z}{\partial\ ln\ T_r}\right]^2$$

Equation (14) can be compared with two similar expressions for gases characterized by van der Waals' equation and Beattie-Bridgeman equation, respectively. They are:

$$\left(\frac{u_c}{u_c^\phi}\right) = \sqrt{\frac{V^2}{(v-b)^2} - \frac{2\,a}{\gamma^\phi\ RTV}}$$

for van der Waals' gas

$$\left(\frac{u_c}{u_c^\phi}\right) = \sqrt{\frac{\gamma}{\gamma^\phi}(1 + 2e_1\rho + 3e_2\rho^2 + 4e_3\rho^3)}$$

for gas obeying Beattie-Bridgeman equation.

Proposed Method of Calculation

It is obvious that a generalized correlation based on the law of corresponding state can be obtained from Equation (12) by plotting u_c^2/T_c against reduced pressure using reduced temperature as parameter for any specified value of C_p^ϕ. The major disadvantage of this approach is that a large number of computations have to be undertaken in order to make this work generalized in the true sense since the heat capacity varies from 5 for a monatomic gas to approximately 40 for a polyatomic gas like C_4F_8. On the other hand, the expression as given by Equation (14) contains four terms: γ^ϕ, C_p, X and Y. While γ^ϕ and C_p are dependent on the molecular structure, X and Y are functions of reduced tempreature and pressure. For this reason, only numerical values of X and Y are presented as generalized charts.

The compressibility information $Z_c = 0.27$ as reported by Lyderson et al[5] serves as the basis for this calculation work. The partial derivatives of Z with respect to T_r and p_r, $\frac{\partial Z}{\partial T_r}$ and $\frac{\partial Z}{\partial p_r}$ first obtained by Slattery and Bird used in their self-diffusion coefficient correlation work[6] were transformed into $\frac{\partial\ ln\ Z}{\partial\ ln\ T_r}$ and $\frac{\partial\ ln\ Z}{\partial\ ln\ p_r}$ and consequently used in the computation of X and Y.

Numerical values of X and Y are presented graphically in Figures 1, 2, 3 and 4, with X (or Y) plotted against P_r with T_r as parameter. The pressure ranges from $p = 0.3$ to 10.0 and temperature from $T_r = 1.0$ to 3.0. All the $X - P_r$ (or $Y - P_r$) curves possess a peak value, its magnitude decreasing and location shifting to the right with the increase of T_r.

The procedure for predicting the critical velocity then becomes fairly simple and straightforward. With the critical properties of the gas known, values of X and Y can be read from the charts directly. Values of C_p^ϕ and γ^ϕ can be obtained either from direct experimental measurements or in case of its absence, can be predicted from spectroscopic data or the empirical group contribution methods suggested by Andersen, Beyer and Watson. The estimation of C_p poses certain problems due to the general unreliability of the information of $C_p - C_p^\phi$. In the work of Lyderson et al the numerical value of $C_p - C_p^\phi$ was obtained by graphically differentiating $(H^\phi - H)/T_c$ with respect to T_r, a process which may introduce large error. It is, therefore, suggested that the direct experimental value of C_p should be used whenever it is available. With all these quantities known, values of u_c/u_c^ϕ and u_c^ϕ can be obtained from Equations (14) and (12) and in turn calculate the value of u_c.

Comparisons

In order to test the accuracy and reliability of this work, critical velocities of carbon dioxide and ethylene near the critical temperature up to the neighbourhood of the critical pressure predicted by this method are compared with the experimental values as reported by Herget[2]. These are shown in Figures 5 and 6.

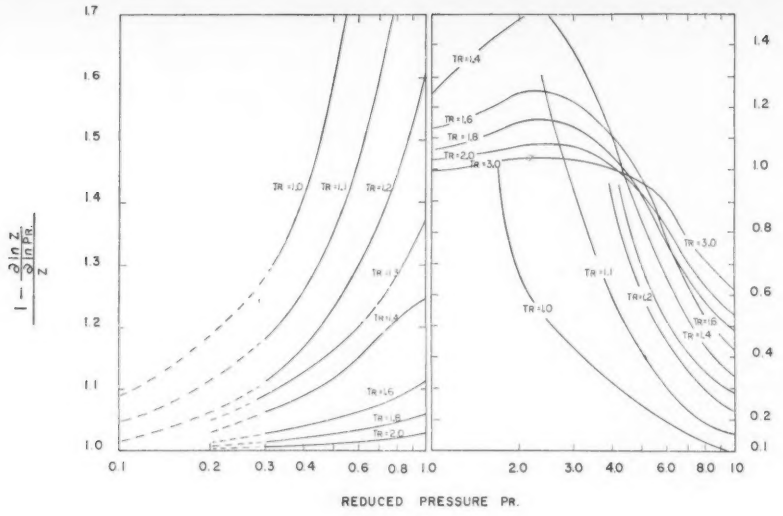

Figure 1.
Generalized Chart No. 1.

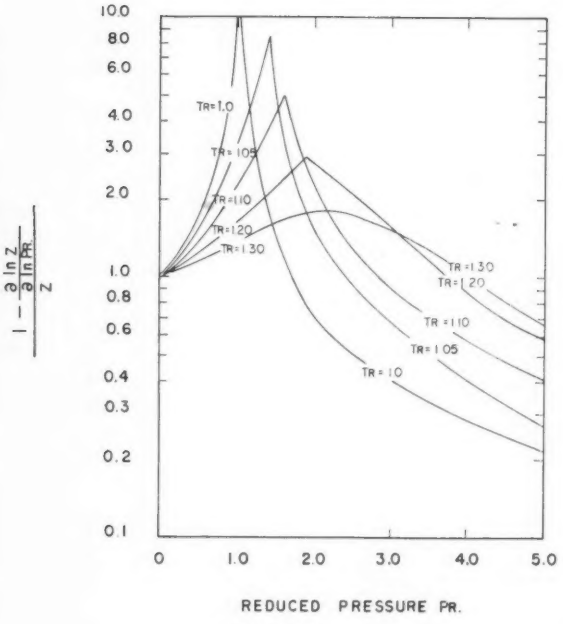

Figure 2.
Generalized Chart No. 2.

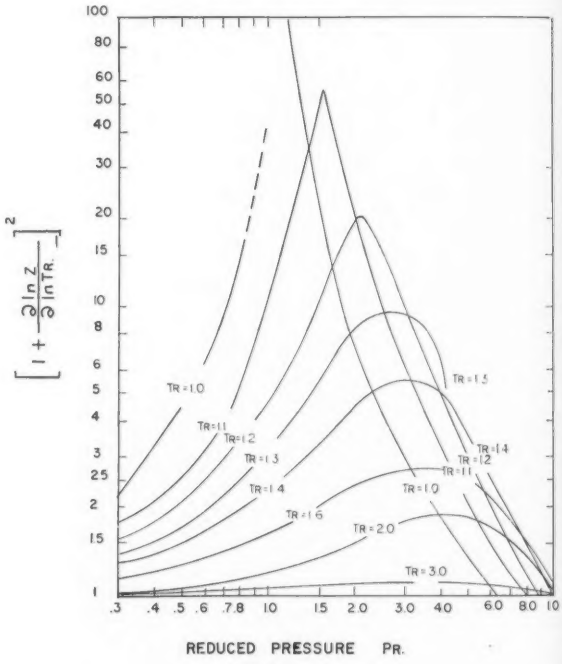

Figure 3.
Generalized Chart No. 3.

For carbon dioxide, the conditions were: $t = 38°C.$ and pressure up to 60 atm. This corresponds to T_r of 1.023 and p_r up to 0.82. The agreement between the predicted and experimental values appear to be fairly good.

In the case of ethylene, a quite different situation arises. The conditions are 9.7°C and pressure up to 60 atm. This gives $T_r = 1.00$ and p_r up to 1.2. The predicted values are consistently lower than the experimental values with a maximum deviation of 54%. However, it should be mentioned that all the pertinent quantities present in Equation (14) approach asymptopically to infinite at $p_r = 1.0$ and, furthermore, the data of $C_p - C_p^\circ$ near the critical point becomes unreliable. This factor might be blamed, at least partly, for the very large deviation.

Acknowledgment

The authors wish to express their thanks to R. B. Bird, University of Wisconsin, Madison, Wisconsin, and J. C. Slattery, Northwestern University, Evanston, Illinois, for providing the numerical values of $\frac{\partial Z}{\partial T_r}$ and $\frac{\partial Z}{\partial p_r}$, which facilitated the computational work.

Nomenclature

C_p° = Heat capacity at constant pressure in ideal state
C_p = Heat capacity at constant pressure
C_v° = Heat capacity at constant volume in ideal state
P = Pressure
R = Gas law constant

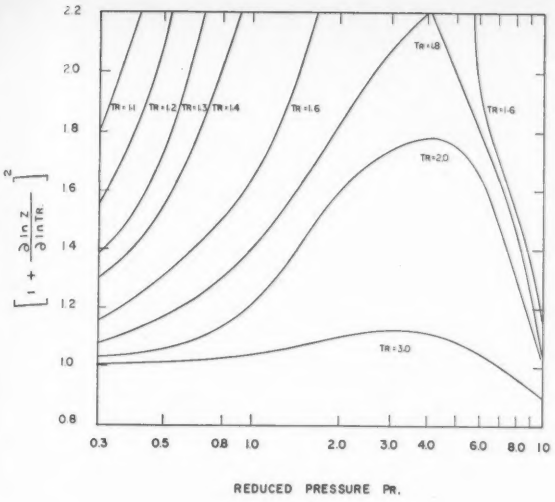

Figure 4.

Generalized Chart No. 4.

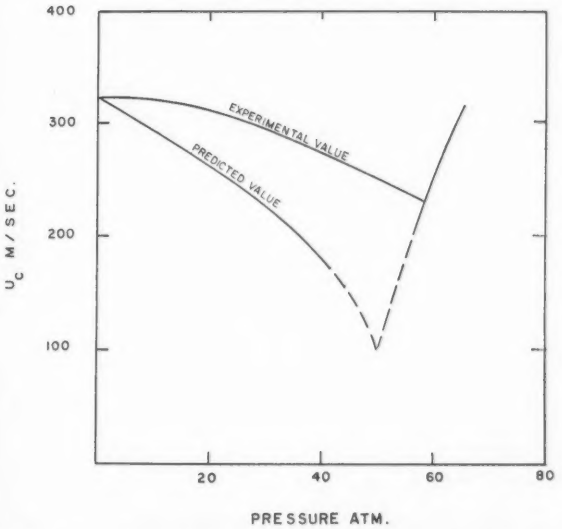

Figure 6 — Comparisons of experimental and predicted value of sound velocity of ethylene at T = 9.7°.

S = Entropy
T = Absolute temperature
U_c = Critical velocity of real gas
u_c^* = Critical velocity of ideal gas

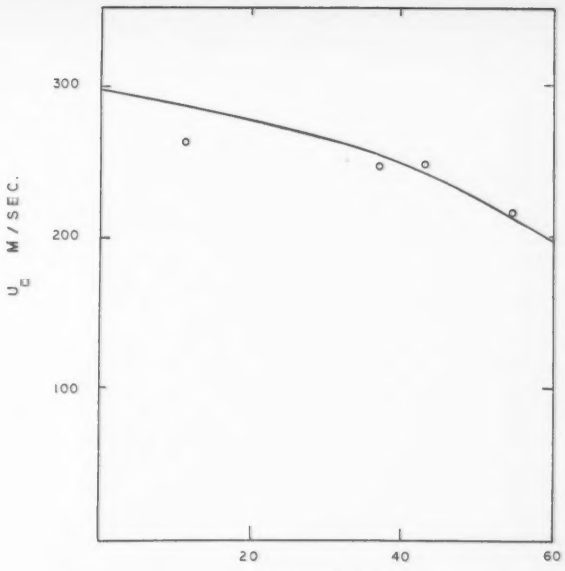

Figure 5 — Comparisons between the predicted and experimental value of sound velocity of carbon dioxide at T = 38°C.

V = Specific volume

X = Dimensionless group, defined as $\dfrac{1-\dfrac{\partial \ln Z}{\partial \ln Pr}}{Z}$

Y = Defined as $\left[1+\dfrac{\partial \ln Z}{\partial \ln T_r}\right]^2$

Z = Compressibility factor
γ^* = Ratio of C_p^* to C_v^*
ρ = Density

References

(1) Donaldson, dup. Colman, and Jones, J. J., NACA TN 2437 (1951).
(2) Herget, C. M., J. Phys. Chem. **8,** 537 (1940).
(3) Tsien, Hsue-shen, Journ. Math. and Phys., **25,** 301 (1947).
(4) Crown, J. C., "Flow of Gas Characterized by the Beattie-Bridgeman Equation of State and Variable Specific Heat: Part I, Isentropic Relations". Naval Ordnance Lab. Memo 9619 (1949).
(5) Lydersen, A. L., Greenkorn, R. A., and Hougen, O. A., "Generalized Thermodynamic Properties of Pure Fluids". Report No. 4, Engineering Experiment Station, University of Wisconsin, Madison, Wisconsin.
(6) Slattery, J. C., and Bird, R. B., A.I.Ch.E. J. **4,** 137 (1958).

★ ★ ★

Salt Effect in Vapor-Liquid Equilibrium, Part II [1]

A. I. JOHNSON[2] *and W. F. FURTER*[3]

Previous work in the field of salt effect in vapor-liquid equilibrium and the theory involved are reviewed briefly. Vapor-liquid equilibrium data at atmospheric pressure are reported for the systems methanol-water, ethanol-water, and n-propanol-water, each saturated with a variety of common inorganic salts. A simple equation is proposed for the representation of salt effect. An attempt is made to ascertain the theoretical significance of this equation, and in so doing, to relate salt effect in vapor-liquid equilibrium to the properties of the system components.

Previous Salt Effect Studies in Vapor-liquid Equilibrium

Limited studies of salt effect on vapor-liquid equilibrium curves were undertaken by Jost[1], Yamamoto[2], Samaddar and Nandi[3], Bogart and Brunjes[4,5], Fox[6], Craven[7], Guyer, Guyer, and Johnsen[8], Butler[9,10], Costa Novella and Tarraso[11], Googin and Smith[12], and Johnson, Furter, and Ward[13].

Other investigators distilled binary mixtures, first alone, and then in the presence of salts, measuring either the distillation rate or degree of enrichment of the overhead product. These were Quartaroli[14,15,16], Kyrides et al[17], and Virtanen[18].

References to salt effect are found in work by Mariller and Coutant[19], Keyes[20], Sunier[21], and Walker et al[22].

Still other investigators drew conclusions from vapor pressure measurements that are related to the subject, those being McBain[23], Wright[24,25,26], Proszt and Kollar[27,28], and Miller[29]. Miller, as early as 1897, stated that the addition of a dissolved salt more soluble in water than in ethanol to aqueous ethanol would result in the depression of the partial pressure of the water and in the elevation of that of the alcohol. The magnitude of salt effect would depend on the difference in the solubilities of the salt in pure water and in pure alcohol. He observed that the total pressure of an ethanol-water mixture at constant temperature was increased by the addition of potassium chloride. Miller concluded that whether the total vapor pressure of a binary system was raised or lowered by salt addition depended merely on whether the partial pressure of one component was lowered more or less than that of the other was raised, this in turn depending on the properties of the components.

[1] *Manuscript received October 19, 1959; accepted February 17, 1960.*
[2] *Associate Professor of Chemical Engineering, University of Toronto, Toronto, Ont.*
[3] *Research Centre, Du Pont of Canada Limited, Kingston, Ont.*
Contribution from the Department of Chemical Engineering, University of Toronto, Toronto, Ont.

Industrial applications of salt effect in vapor-liquid equilibrium were reported by Bogart and Brunjes[4,5], Gorhan[30], Dittmar[31], Morrell and Gilliland[32], and Kelly[33].

Some of the best previous work in the field was carried out by Garwin[34], Reider and Thompson[35], Tursi and Thompson[36], and Fogg[37]. However, in only the latter two investigations were even empirical correlations attempted. These are reviewed elsewhere[38].

In general, the previous work in the field of salt effect in vapor-liquid equilibrium has been rather uncertain in nature and tending to lack in fundamental approach. Doubts have been voiced over the validity of many of the data. Little but qualitative observations confirming the early work of Miller have been drawn.

Previous Salt Effect Studies in Liquid-liquid Equilibrium

"Salting out" is used generally to denote a decrease in the solubility of the nonelectrolyte in the solution, or, more rigorously, an increase in its activity coefficient, caused by the salt addition. "Salting-in" refers to the opposite case.

The complete literature on salting in and out in liquid solutions has been reviewed comprehensively by Long and McDevit[40]. They indicate that the standard method of correlating salt effect is to represent the logarithm of the activity coefficient of the nonelectrolyte as a power series in the concentrations of all solute species (salt and nonelectrolyte) at constant temperature and pressure, assuming the solvent to be a structureless dielectric continuum and all deviations from ideality being due to electrostatic interaction alone. Only the linear terms are retained, assuming moderate solute concentrations. The result is the limiting relation

$$\log \gamma_{2_s} = k_{32} N_3 + k_{22} N_2 \quad \ldots\ldots\ldots\ldots (1)$$

in which components 1, 2, and 3 represent water, nonelectrolyte, and salt respectively.

Salt effect theories are generally concerned with the calculation of k_{32}, the ion-nonelectrolyte interaction parameter, and not with k_{22}, the nonelectrolyte self-interaction parameter. The usual units are either molarity or mole fraction. The quantity of k_{32} is known as the "salting out parameter" and is commonly used to indicate magnitude of salt effect. Negative values of k_{32} indicate the occurrence of the opposite effect, salting in. Electrolyte dissociation must be considered when attempting to place salts in order of effectiveness. If molecular values are used for N_3, the salt parameter then includes consideration of ionic charges and the number of ions per salt molecule. This equation has been found successful even at quite high salt concentrations[40].

The causes and effects of the preferential attraction of a dissolved salt for one component of a water-nonelectrolyte solution over the other have been explained in various salt effect theories, some quantitative but most qualitative. These attempts can be classified under one of the following: hydration, electrostatic interaction, van der Waal's forces, and internal pressure. They are discussed at length by Long and McDevit[40].

The electrostatic theories of Debye and McAuley[41], Kirkwood[42], and others, while giving the only really quantitative approach to salt effect, yield only limiting laws because of their restrictive assumptions. They do indicate that the logarithm of the activity coefficient of the nonelectrolyte is proportional to the ionic strength (and hence mole concentration) of the salt in the limiting case of infinite dilution. At finite electrolyte concentrations the electrostatic field of an ion would be expected to be weakened by ion interaction. Furthermore, the parameters involved in applying these equations are often difficult to evaluate. Altshuller and Everson[43] state that experimental measurements of dielectric constants of electrolytic solutions have been confusing and contradictory. They also state that ionic radii obtained crystallographically do not apply with exactness in solution. Mean ionic radii and distances of closest approach are nebulous properties, difficult to evaluate. The literature contains few data on the effect of nonelectrolyte concentration on dielectric decrement. The electrostatic theories have been unsuccessful generally in predicting the salting out parameter k_{32}.

Continuing in the simplified behavior pattern suggested by Gross[39], salting in would indicate a preferential attraction of ions for the nonelectrolyte over the solvent, even when the nonelectrolyte is less polar. The larger the ion, the lesser its electrostatic field. In the presence of either undissociated salt molecules or large ions, (the case in point is mercuric chloride), the highly polar water molecules would tend more towards orienting into an associated state with each other than with the salt, forcing the salt particles into the vicinity of the less polar nonelectrolyte molecules. The large ion, attracted to a nonelectrolyte molecule, would result in the formation of an ion-nonelectrolyte association.

Since no one theory has been able to represent satisfactorily the data on salt effect in the liquid phase except in restricted and limiting cases, previous investigators in general agreed that salt effect is caused by a complexity of forces and interactions, no one of which is sufficiently insignificant in relation to the others that it may be neglected.

THEORETICAL PRINCIPLES

The effect of a salt, when added to a solution of two liquid components, is to alter the composition of the equilibrium vapor phase. Alterations in properties such as vapor composition and total pressure or boiling temperature caused by the salt addition are outward manifestations of the effect of the salt on the more fundamental properties of the two volatile components, their chemical potentials.

Salt Effect on Chemical Potential

Consider a two-component, two-phase system in which both components appear in both liquid and gaseous phases. It will be designated by lack of subscript. To this system is added a non-volatile dissolved salt which appears only in the liquid phase. This latter system will be designated by the subscript "s".

Assume the number of molecules present in the vapor phase to be sufficiently small compared to the liquid that a change in vapor composition will not alter the ratio of the two volatile components in the liquid. Assume equilibrium to exist in each of the two systems described above.

Butler[9,10] pointed out that the preferential attraction of the added ions for one volatile component over the other removes molecules of the former component from their solution role. This decreases their activity in the main body of the solution. Molecules of the other component are expelled from the ionic regions into a greater activity in the solution. He indicated that the net result was a reduction in the chemical potential of the former component and an increase in that of the latter.

It would therefore be rational to seek a correlation for salt effect in vapor-liquid equilibrium in the altering of the chemical potentials of the two volatile components by the salt.

Define a measure of salt effect as:

$$\text{effect} = (\mu'_{2s} - \mu'_2) - (\mu'_{1s} - \mu'_1) \quad \ldots\ldots (2)$$

Assume the vapor phase to be an ideal gaseous solution. Hence

$$\mu'_i = F_i^\circ + RT \log y_i \pi \quad \ldots\ldots (3)$$

Assuming at constant pressure, that the salt addition has a negligible effect on the temperature of the boiling system, substitution of Equation (3) into Equation (2) yields

$$\text{effect} = RT \log \frac{y_{2s}\, y_1}{y_2\, y_{1s}} \quad \ldots\ldots (4)$$

Since the values of n_1 and n_{2s} and hence of x_2 have not been altered by salt addition,

$$\text{effect} = RT \log \frac{\alpha_s}{\alpha} \quad \ldots\ldots (5)$$

Since the system variables are pressure, temperature, and the amounts of the components, and since pressure, temperature and the amounts of the two volatile components in the liquid phase are fixed, the above quantity suggests itself for relating salt effect on the vapor phase to salt concentration in the liquid.

$$T \log \frac{\alpha_s}{\alpha} = f(N_3) \quad \ldots\ldots (6)$$

Assume a linear relationship as a first approximation.

$$T \log \frac{\alpha_s}{\alpha} = C\, N_3 \quad \ldots\ldots (7)$$

Reduction of Gilliland's Equation

Gilliland[44], using ternary van Laar equations, established that the effect of the addition of a volatile, nonelectrolytic, liquid third component to the vapor-liquid equilibrium of a binary system was

$$T \log \frac{\gamma_2'/\gamma_1'}{\gamma_2/\gamma_1} = \phi\, V_3 \quad \ldots\ldots (8)$$

where ϕ is a function of the ternary van Laar coefficients.

In the nomenclature of the present investigation, and making the same assumption that the temperature of the boiling system has not been altered materially at constant pressure by the third component addition, the above equation reduces to

$$T \log \frac{\alpha_s}{\alpha} = f(N_3)$$

which is similar to Equation (6), although derived for nonelectrolyte third components from van Laar equations.

Assumption of Constant Temperature

If Equation (7) is to be applied in evaluating the effect of salt concentration on the vapor-liquid equilibrium relationships of a boiling system at various solvent-nonelectrolyte ratios, the existence of a relatively narrow boiling temperature range would permit the assumption of constant temperature. In this case, Equation (7) reduces to

$$\log \frac{\alpha_s}{\alpha} = k_3\, N_3 \quad \ldots\ldots (9)$$

where k_3 is an empirical quantity representing the over-all specific effect of a given salt on the vapor-liquid equilibrium of a given binary system.

Relation of Salting Out Parameter to Vapor-liquid Equilibrium

The effect of salt concentration on the activity coefficient of the nonelectrolyte (alcohol) is represented generally by the approximate Equation (1).

Applying the boundary conditions that at $N_3 = O$, $\log \gamma 2s = \log \gamma 2$, this expression becomes

$$\log \frac{\gamma_{2s}}{\gamma_2} = k_{32}N_3 \quad \ldots\ldots(10)$$

Similarly

$$\log \frac{\gamma_{1s}}{\gamma_1} = k_{31}N_3 \quad \ldots\ldots(11)$$

At constant temperature pressure, and n_1 and n_2,

$$\frac{\alpha_s}{\alpha} = \frac{y_{2s}y_1}{y_{1s}y_2} = \frac{P_2^\circ \gamma_{2s}N_{2s}\, P_1^\circ \gamma_1 N_1}{P_1^\circ \gamma_{1s}N_{1s}\, P_2^\circ \gamma_2 N_2} =$$

$$\frac{\gamma_{2s}\gamma_1}{\gamma_{1s}\gamma_2} \cdot \frac{\dfrac{n_2}{n_1+n_2+n_3} \cdot \dfrac{n_1}{n_1+n_2}}{\dfrac{n_1}{n_1+n_2+n_3} \cdot \dfrac{n_2}{n_1+n_2}} = \frac{\gamma_{2s}\gamma_1}{\gamma_{1s}\gamma_2} \quad \ldots\ldots(12)$$

Combination of Equations (10), (11), and (12) yields

$$\log \frac{\alpha_s}{\alpha} = (k_{32} - k_{31})N_3 \quad \ldots\ldots(13)$$

where k_{32} is the ion-nonelectrolyte parameter used by previous investigators to measure salting in and out and k_{31} would similarly represent ion-solvent interaction.

Equations (9) and (13) are identical when

$$k_3 = k_{32} - k_{31} \quad \ldots\ldots(14)$$

Cancelling-out of Terms

Equation (9), which has been arrived at from three different directions, postulates a linear relationship between the quantities involved only for a constant solvent-nonelectrolyte composition ratio. It has been argued that salt effect is a complex function of interactions and self-enteractions between all three components. In addition, the degree of dissociation of salts in aqueous alcohol is known to vary with the water-alcohol ratio. Therefore, no theory exists to indicate that the value of k_3 should be expected to remain constant for a given system as the binary liquid composition is varied.

It is evident from Equations (10) and (11) that in the absence of simplifying assumptions they should have additional terms. This fact becomes more apparent when Equations (10) and (11) are derived from definitions of the activity coefficient and the "Gibbs characteristic"[45].

However, it is conceivable that these interactions may either not vary appreciably, or, more likely, tend to balance each other, as the solvent-nonelectrolyte ratio is varied. Should this prove to be the case, then the additional terms of Equations(10) and (11) would tend toward cancelling each other. Since Equation (9) represents the difference between equations (10) and (11), such a cancelling tendency would permit Equation (9) to represent a vapor-liquid equilibrium curve, and to represent it even in cases when Equations (10) and (11) failed altogether for varying values of x_2.

Correlation and Prediction

Having established the value of k_3, and knowing the vapor-liquid equilibrium data for the binary system free of salt, Equation (9) would permit the calculation of salt effect on vapor-liquid equilibrium, should it be found to apply.

For any value of x_2, the equation would relate salt concentration to vapor composition. It would predict the vapor-liquid equilibrium curve for any given salt concentration or calculate the amount of salt necessary for a desired vapor enrichment.

In addition, if salt solubility as a function of binary liquid composition is known or can be estimated, this equation would predict the equilibrium curve for saturated salt concentration from the salt solubilities in the two pure components. This latter curve would represent the maximum effect possible from a given salt, this maximum effect being a function not only of the salt effect parameter but also of the solubility of the salt.

EXPERIMENTAL METHOD

A primary purpose for establishing the binary vapor-liquid equilibrium data of the three alcohol-water systems was to compare these data to those in the literature as a check on the accuracy of the apparatus and experimental method. The data for the ethanol-water system at atmospheric pressure were reported in Part I of this series[51]. Those for methanol-water and n-propanol-water, along with a comparison with literature data, are included in this paper. The method is that described in Part I. In addition, in each run with these three binary systems, the steady state liquid composition, calculated by material balance from the volumes and densities of the charge to the still and the steady state condensed vapor holdup in the condensate chamber, was compared to the actually measured value at the end of the run. This was a check on the material balance method used to obtain the equilibrium liquid composition on a salt-free basis in the presence of saturated salt.

The data for these two systems are reported in Tables 1 and 2. Figures 1 and 2 illustrate these data. Averages of the best literature data on methanol-water[44,46,47,48,50,52,53,54] and n-propanol-water[44,46,48,49] are shown as solid lines in these figures, while the points represent the experimental data reported in the tables.

The alcohols and salts used in the investigation were of analytical reagent grade. Their exact specifications are listed with the original data[38].

The vapor-liquid equilibrium data for the alcohol-water-salt systems were obtained with the apparatus and method described in Part I. For some of the systems, saturated salt concentrations were measured by Mohr titration for chloride ion, while for others the concentration was merely reported as being saturated. The steady state liquid composition was calculated by material balance from the volumes and densities of the liquid charged to the still before the addition of salt and of the steady state condensed vapor holdup, compositions being obtained by specific gravity measurement of samples.

EXPERIMENTAL RESULTS

The experimental data for the alcohol-water binary systems checked with the averaged literature data to about two-tenths of one mole per cent. The comparison between steady state liquid compositions actually measured and those determined by material balance showed an average deviation of less than one-tenth of one mole per cent, indicating the system to be closed and the material balance method a suitable technique.

Tables 1 and 2 list the experimental data for methanol-water and for n-propanol-water and Tables 3 to 26 list the vapor-liquid equilibrium data at atmospheric pressure for 24 alcohol-water saturated systems, the compositions being reported on a salt-free basis. Tables 27 and 28 report additional data for the systems methanol-water-ammonium chloride and methanol-water-calcium chloride in which for each of several liquid compositions on a salt free basis, salt concentration was varied

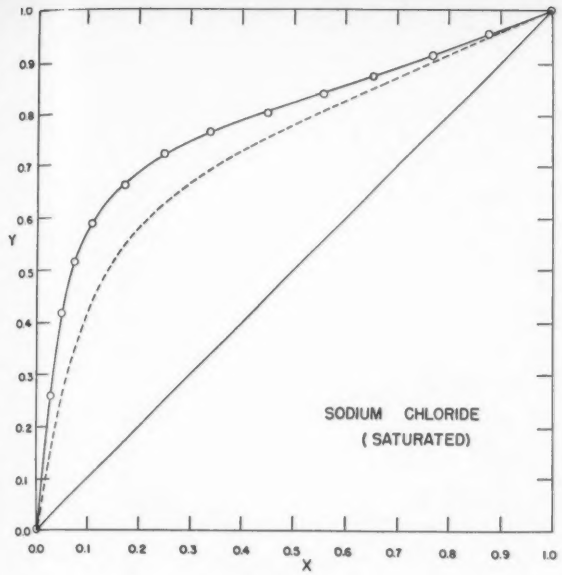

Figure 1.

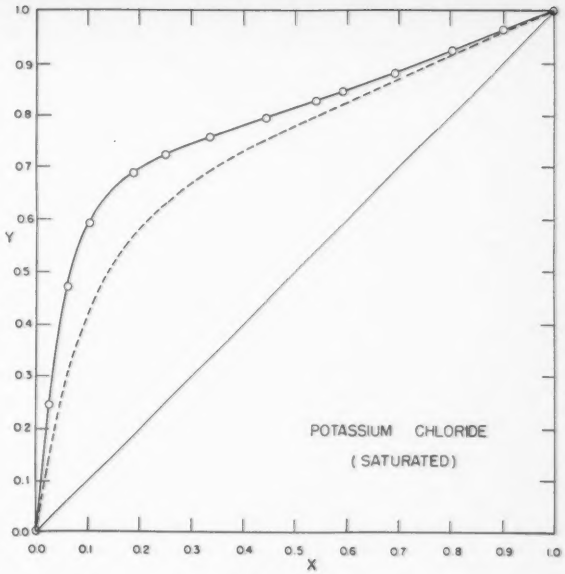

Figure 2.

Typical liquid-vapor equilibrium curves for methanol-water with salt effect (atmospheric pressure).

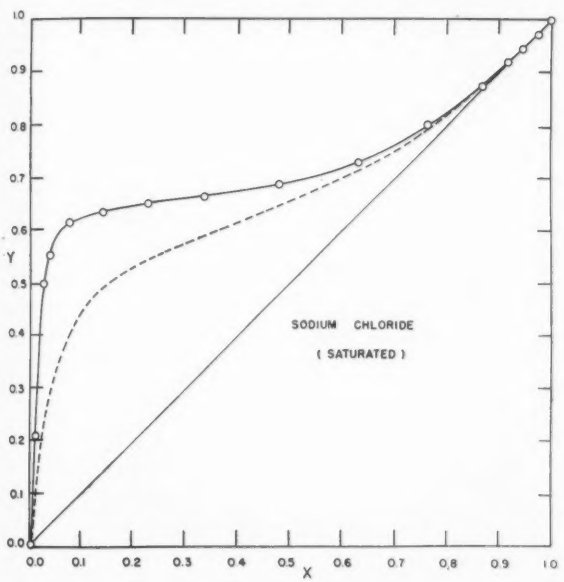

Figure 3.

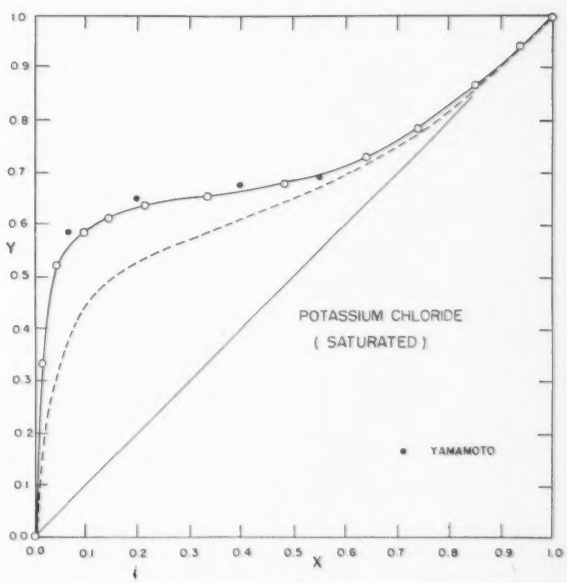

Figure 4.

Typical liquid-vapor equilibrium curves for ethanol-water with salt effect (atmospheric pressure).

and its effect on vapour composition noted. Complete tabulated data are obtainable from the American Documentation Institute.*

Figures 1 to 8 illustrate some of the typical vapor-liquid equilibrium curves. The curves are for atmospheric pressure and are reported on a salt free basis. The curve for the corresponding alcohol-water system without salt is shown on each figure as a dashed line for comparison purposes, in order that the magnitude of the salt effect may be seen readily. Literature data are included on these graphs for the systems for which any exist. Complete graphs may be seen in the original thesis.[38]

*Tables 1 to 28 of this paper have been deposited as Document No. 6256 with the ADI Auxiliary Publications Project, Photoduplication Service, Library of Congress, Washington 25, D.C. A copy may be obtained by citing the Document No. and by remitting $1.25 for photoprints, or $1.25 for 35 mm. microfilm. Advance payment is required. Make cheques or money orders payable to: Chief, Photoduplication Service, Library of Congress.

DISCUSSION OF RESULTS

Although most salts salted out alcohol from water in the three alcohol-water binary systems investigated, as is evidenced by the increased activity of alcohol in the vapor phase, some had little effect because of low solubility. Two salts, mercuric chloride and mercuric bromide, caused salting in as illustrated in Figure 8. The occurrence of this latter effect results in negative values of k_3.

Some very slight shift of the ethanol-water azeotrope to a composition richer in ethanol apparently is caused by those salts most effective at salting out ethanol. This effect is indefinite because the solubility of these salts in the azeotropic mixture is so low that salt effect is almost nonexistent. As shown in Figures 5 and 6 these salts do cause marked azeotrope shifts

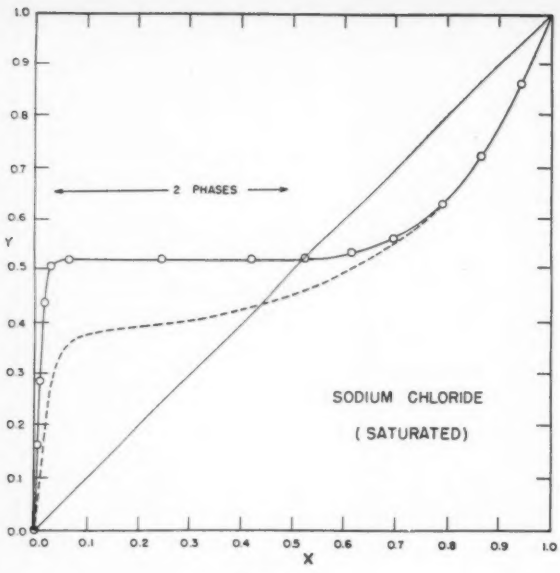

Figure 5.

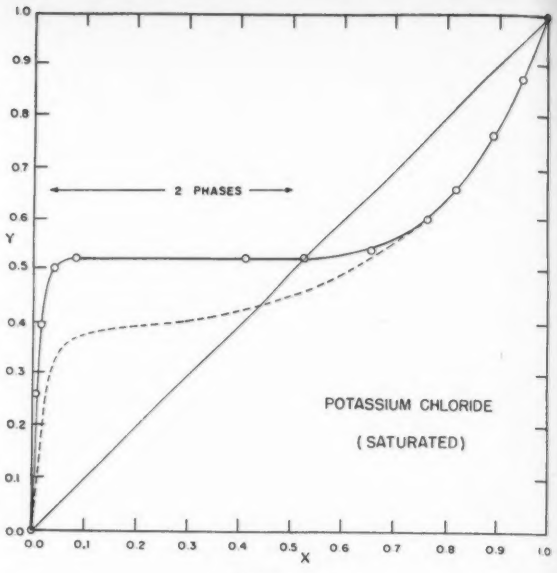

Figure 6.

Typical liquid-vapor equilibrium curves for n-propanol-water with salt effect (atmospheric pressure).

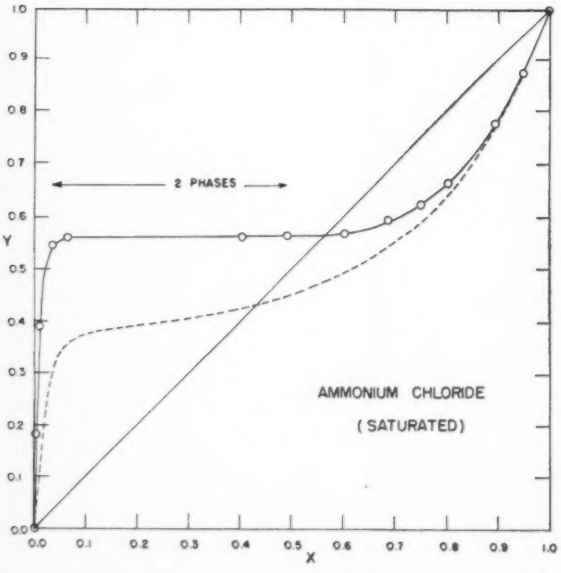

Figure 7—Liquid-vapor equilibrium data for n-propanol-water with ammonia chloride (atmospheric pressure).

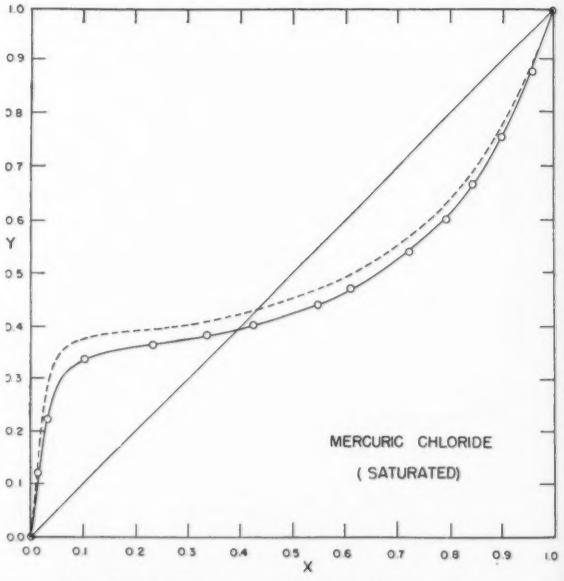

Figure 8—Liquid-vapor equilibrium data for n-propanol-water with mercuric chloride (atmospheric pressure).

in the n-propanol-water system because of the higher salt solubility in the more water-rich azeotropic composition. Mercuric chloride (Figure 8), being quite soluble in the azeotropic regions of both systems, causes a substantial shift in the other direction owing to its salting in effect.

Most of the salts that caused salting out of the alcohols were much more soluble in water than in the alcohols. Since, at saturated salt concentrations, salt effect is a function of its solubility in the system, the large salt effect in the water-rich regions, which tends to diminish rapidly as liquid composition moves toward the alcohol-rich region, is explained. The shape of the solubility curve also explains why salts such as mercuric chloride, which are quite soluble in both components, exert a more uniform effect throughout the binary composition range. The former effect is characterized by a small fractional value of the exponent in Equation (15), and the latter by a value closer to unity.

Examination of the data shows the boiling ranges of the systems investigated to be quite narrow over most of their liquid composition ranges. When this range width is compared to the approximate absolute temperature, the fractional variation would appear sufficiently small to justify the assumption of constant temperature. Examination of the data also shows that boiling point elevations and depressions caused by the salts are quite small, usually a degree or less.

Experimentally, saturation was assumed to exist when a slight excess of solid salt persisted over a period of time. All salts employed in the investigation dissolved quite rapidly.

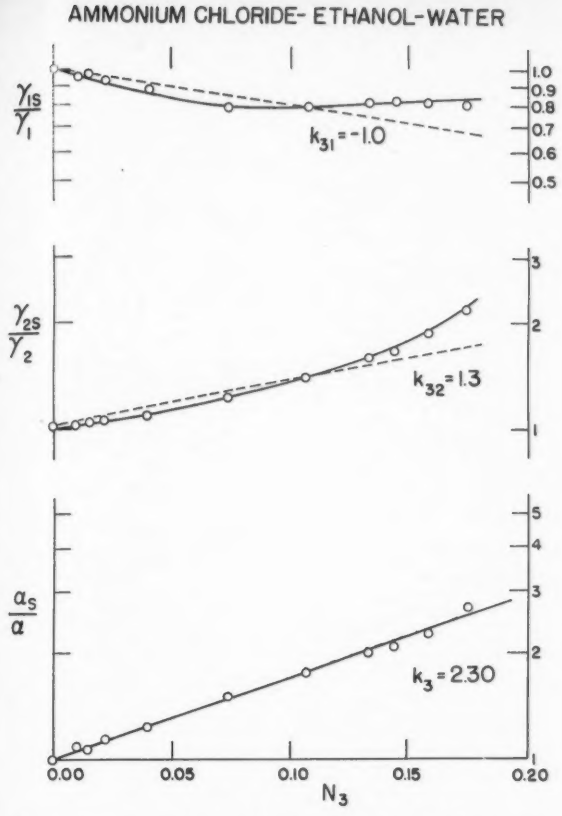

Figure 9 — Typical calculated data showing interaction parameters and correlation constant.

Furthermore, the system was saturated with salt under conditions of zero vapor condensate holdup. The establishment of a holdup after first approaching saturation further ensures its attainment by removing some salt-free liquid from the salution as vapor to create this holdup.

Because of the material balance technique of establishing the equilibrium liquid composition, salts known to possess hydrated forms at the conditions of temperature and pressure involved were avoided generally. (The slight excess of solid salt present to ensure saturation, by becoming hydrated or alcoholated, would alter liquid composition.)

In some systems the salting out effect was of such magnitude as to cause a reduction of mutual solubility to the point of formation of two liquid phases as illustrated in Figures 6 and 7. This effect becomes more probable as the alcohol series is ascended and the alcohol-water mutual solubility is less.

An advantage of analysis of equilibrium liquid composition by material balance occurs in systems in which the salt causes formation of a region of two liquid phases. Since the binary charge is analysed before the salt is added, this method permits the calculation of over-all liquid composition at steady state, a quantity very difficult to measure otherwise. In the region of two liquid phases, the phase rule indicates that zero degrees of freedom exist, a fact confirmed by the horizontal slope of the equilibrium curve. In this region the compositions of the vapor and two liquid phases are fixed and only the relative amounts of the two liquid phases can be varied.

TREATMENT OF EXPERIMENTAL RESULTS

(a) In Tables 27 and 28 data are reported for two systems in which x_2 was held constant at each of several values while salt concentration was varied. As shown in Figure 9(c) the data for each value of x_2 were plotted as per Equation (9) and the values of k_3 established. From these values of k_3, the known salt-free binary equilibrium data, and the experimentally measured values of x_2 and N_3, Equation (9) was employed to calculate vapor enrichments. These calculated values of y_2 were compared to the experimentally determined values. The over-all average numerical deviation for the 37 experimental points of these two systems was 0.003 mole fraction. For a given system, the value of k_3 was observed to be almost independent of x_2.

(b) Data are reported for 24 systems consisting of alcohol-water-saturated salt. In 9 of these systems, saturated salt concentrations were actually measured. For each of these 9 systems, the data were plotted as per Equation (9) and a straight line drawn to determine the best single value of k_3 for the system. As above, Equation (9) was then used to calculate vapor compositions, which were then compared to the experimental values. The over-all average numerical deviation for the 116 experimental points of these 9 systems was 0.009 mole fraction.

In addition, as illustrated by Figures 9(a) and 9(b), activity coefficients were calculated from the data, and these data were plotted as per Equations (10) and (11) for the purpose of examining any tendency toward the proposed cancelling-out effect. Table 29 lists the values of the parameters obtained from these plots. Values of k_{31} and K_{32} are reported to only two figures because of the apparent non-linearity of the data with Equations (10) and (11). The additivity expressed in Equation (14) is to be noted.

(c) Providing the relation between salt solubility and binary composition is known, Equation (9) is proposed to predict the vapor-liquid equilibrium curve of a system from a knowledge of only the solubility of the salt in each of the two pure volatile components.

Curves of S_3 against x_2 were plotted for the nine systems for which saturated salt concentration data had been measured, the intercepts representing the salt solubility in the two pure components. These curves indicated that a relatively large amount of the component in which the salt is more soluble is required to change the salt solubility appreciably from its value in the component in which it is less soluble. This effect is great with large solubility differences of the salt between the two components and small when the difference is little. In other words, the solubility curves were festoon-like in shape.

Because of the complexity of the various solution phenomena governing the solubility of an electrolyte across the entire composition range of a boiling binary solvent under constant pressure conditions, an empirical solubility relation was chosen. The configuration of the measured solubility curves suggested the following relation:

$$S_3 = (S_{32} - S_{31})\, x^d + S_{31} \qquad (15)$$

where S_{31} and S_{32} are the intercepts of the S_3 versus x_2 curve and represent the salt solubility in the pure components. The values, taken from Seidell[55], of salt solubilities at x_2 values of 0, 0.5 and 1 were used to evaluate the constant d for each system. The values of S_{31} and S_{32} were taken at a single temperature for each system, this temperature representing the average boiling temperature of the system. The value of k_3 was calculated for each of the 24 systems from a single experimental point of each system. The values used are contained in Table 30. (The reason for k_3 differing for a given system between Tables 29 and 30 lies in this single temperature at which values of S_{31} and S_{32} were taken from the literature.)

From the known salt-free binary vapor-liquid equilibrium curve and the values of N_3 calculated from S_3 (in turn calculated from Equation 15), the saturated salt vapor-liquid equilibrium curve was predicted with Equation (9) for each of the 24 systems at x_2 values from 0 to 1 in 0.1 increments. The calculated vapor compositions were compared to those taken from the experi-

TABLE 29

TABULATED INTERACTION PARAMETERS

System	k_{31}	k_{32}	k_3
methanol – water – sodium chloride	−1.2	1.9	3.12
ethanol – ,, – ,, ,,	−1.2	2.4	3.56
n-propanol – ,, – ,, ,,	−1.2	4.0	5.18
methanol – water – potassium chloride	−1.0	2.3	3.38
ethanol – ,, – ,, ,,	−1.0	2.4	3.40
n-propanol – ,, – ,, ,,	−1.0	3.1	4.16
methanol – water – ammonium chloride	−1.0	0.7	1.75
ethanol – ,, – ,, ,,	−1.0	1.3	2.30
n-propanol – ,, – ,, ,,	−1.0	1.8	2.83

mentally determined curves. The over-all average deviation for the 264 point of these 24 systems was 0.005 mole fraction.

The detailed calculations and comparisons outlined above are presented more fully elsewhere[38].

DISCUSSION

Representation of Data

Equation (9) was found to represent salt effect on vapor-liquid equilibrium successfully when salt concentration was varied at constant x_2. Carrying this out at various fixed values of x_2 for a system, the quantity k_3 was found to be relatively independent of binary liquid composition.

This observation was further confirmed in the ability of Equation (9) to represent the data for the nine systems in which salt concentrations were measured, using a single value of k_3 over the entire liquid composition range of each system. Furthermore, for the 24 systems tested, because saturated salt concentration as a function of liquid composition and temperature was capable of being approximated, the equation allowed prediction of the effect on the vapor-liquid equilibrium curve of saturating the system with salt, from a knowledge of the basic solubility properties of the components. The representation of the data by Equation (9) was accurate to a deviation of the order of one mole per cent or less, these deviations including any experimental inconsistencies in the unsmoothed data.

Cancelling-out Effect

The observed lack of change in the value of the function of k_3 across the liquid composition range of a system would indicate the existence of a balancing tendency, or cancelling-out of opposing effects, among the various effects comprising the action of a salt on vapor-liquid equilibrium.

An examination of the plots of activity coefficient and relative volatility ratios against salt concentration as per Equations (9), (10), and (11) for the nine systems indicates clearly that Equation (9) tends to represent these data linearly while Equations (10) and (11) do not. Figure 9 is included as a sample illustration of one of these systems. It may be seen from these plots that, for each value of salt concentration, the activity coefficient ratio of the water tends to deviate in the same direction from a best straight line as does the activity coefficient ratio of the alcohol. Since Equation (9) represents the difference between Equations (10) and (11), these deviations tend to cancel, enabling Equation (9) to hold adequately over the entire vapor-liquid equilibrium curve of a given system with a single value of k_3.

Prediction of Salting Parameters

Although Equations (10) and (11) reduce in the limiting case of infinite dilution of one of the volatile components to Raoult's Law, attempts to calculate k_{31} and k_{32} from vapor pressure depression data were unsuccessful, since it was found that the limiting values so obtained did not approximate the values in the presence of the second volatile component. For these systems it has been necessary to establish the value of k_3 from a single experimental determination per system.

Raoult's Law predicts that the salt would lower the vapor pressure of each volatile component in the absence of the other. Hence the limiting values of k_{31} and k_{32} in the absence of the other volatile component would be expected to be negative. However, when salt is added to a mixture of the two volatile components, the salt, in salting out one component, actually *raises* its partial pressure while lowering that of the other. The difference between the effect of the salt on a component alone and on that component in the presence of the other would then be an indication of the relative importance of the *other* in determining the total salt effect in the mixture.

TABLE 30

TABULATED SOLUBILITY DATA AND CORRELATION CONSTANTS

System	S_{31}	S_{32}	d	k_3
methanol – water – ammonium chloride	0.217	0.025	0.4	2.4
,, – ,, – sodium chloride	0.117	0.005	0.4	3.8
,, – ,, – potassium chloride	0.124	0.003	0.3	4.3
,, – ,, – sodium nitrate	0.310	0.005	0.4	2.5
,, – ,, – lead nitrate	0.059	0.000	0.3	2.0
,, – ,, – mercuric chloride	0.018	0.233	1.0	−0.9
ethanol – ,, – ammonium chloride	0.225	0.000	0.3	3.6
,, – ,, – sodium chloride	0.118	0.000	0.3	4.8
,, – ,, – potassium chloride	0.125	0.000	0.3	4.2
,, – ,, – sodium nitrate	0.320	0.000	0.3	3.0
,, – ,, – lead nitrate	0.061	0.000	0.3	3.5
,, – ,, – mercuric chloride	0.021	0.160	1.0	−0.6
,, – ,, – mercuric bromide	0.002	0.077	1.0	−0.9
,, – ,, – mercuric iodide	0.007	0.005	1.0	0.1
,, – ,, – barium nitrate	0.019	0.000	0.3	2.0
,, – ,, – potassium sulphate	0.022	0.000	0.2	1.0
,, – ,, – ammonium sulphate	0.129	0.000	0.1	3.5
,, – ,, – cuprous chloride	0.010	0.000	0.3	2.4
n-propanol – ,, – ammonium chloride	0.242	0.000	0.3	3.5
,, – ,, – sodium chloride	0.120	0.000	0.2	6.9
,, – ,, – potassium chloride	0.134	0.000	0.2	6.3
,, – ,, – sodium nitrate	0.350	0.000	0.4	2.7
,, – ,, – lead nitrate	0.078	0.000	0.2	4.0
,, – ,, – mercuric chloride	0.029	0.088	1.0	−0.9

Therefore the departure of the salt-water interaction parameter k_{31} from a negative value could be considered a measure of the relative significance of salt-alcohol interaction in determining salt effect, and the departure of the salt-alcohol interaction parameter k_{32} from a negative value a measure of salt-water interaction significance.

The salts ammonium, sodium, and potassium chloride salted out the three alcohols under study from aqueous solution quite strongly. The values of k_{31} were observed to be negative, while those of the salting out parameter k_{32} were changed to substantial positive values. This would indicate that salt effect is strongly governed in the above examples by ion-water interactions and only by ion-alcohol interactions. This fits well with the picture of the strong affinity of the ions of these three salts for highly polar water molecules, in effect repelling the less polar alcohol molecules from the ionic regions of the solution and removing them from close contact with the ions.

Relation of Salt Effect in Vapor-liquid Equilibrium to Salting In and Out in Liquid Solutions

Salting out of a non-electrolyte in liquid solution has been explained by the fact that the ions exert a preferential attraction for the molecules of one volatile component over those of the other. The former are drawn into associations with the ions, reducing their activity in solution. The latter are expelled from the ion regions into a greater activity in the body of the solution remote from the ions.

Because of the electrostatic field of the ions and its attraction for these molecules, the volatility of the regions consisting of ion-molecule complexes is abnormally low. Hence the vapor composition is determined mainly by the solution regions remote from the ion fields (rather than by the over-all liquid composition as would be the case in the absence of the salt). Since the portion of the liquid from which most of the vapor arises has been increased in the less-attracted component, the net result is an altering of the equilibrium vapor composition. The increased activity of this latter component in solution is reflected by its increased partial pressure in the vapor while the partial pressure of the more-attracted component is reduced by the salt addition.

Reduction of Mutual Solubility

As a general rule, the degree of solubility of one substance in another depends on the degree of similarity between the molecules of the two substances. Like things tend to dissolve in each other. When ions are added to a solution of two volatile nonelectrolytes and they exert a preferential attraction for one component over the other, they enter into associations with this component. By so doing, they reduce the degree of similarity between the two components. This is offered as a simple qualitative explanation of the reduced mutual solubility that is salting out.

Relation of Salt Solubility to Salt Effect

(a) Previous investigators have noted qualitatively that a salt more soluble in the less volatile component than in the more raises the relative volatility of the system and vice versa.

The relation of salt solubility to its attraction for a component is postulated as the explanation for this observation. Since like things tend to dissolve like, ionic substances such as potassium chloride would be expected to be more soluble in polar water than in less polar alcohols. In other words, as a general rule, the salt would be more soluble in the component for which it exerts a greater attraction in solution.

The salt, having a lesser attraction for the component in which it is less soluble, salts out this component, hence raising its volatility in relation to that of the other. If the component in which the salt is less soluble is the more volatile, the relative volatility of the system is raised, and vice versa.

Since salt effect is governed by the degree of difference between the attraction of the salt for one component over the other, the above postulate also explains why the magnitude of salt effect has been observed to be a function of the difference between the solubilities of the salt in the two pure components.

(b) For cases in which salts exhibit festoon-like solubility curves with liquid composition, a development similar to that of Gordon[56] will yield a more rigorous basis for the relation of salt solubilities in the two pure components to salt effect in vapor-liquid equilibrium at saturation.

For the purpose of the following argument only, assume that Component 1 is the component in which the salt is more soluble, and that T, P, and n_1 are held constant. When the saturated salt is in equilibrium with a slight excess of solid salt (i.e. its chemical potential is constant) expansion of the derivative of the chemical potential of the salt in its variables reduces to

$$\left(\frac{\partial \mu_3}{\partial n_3}\right)_{n_1,n_2} . dn_3 + \left(\frac{\partial \mu_3}{\partial n_2}\right)_{n_1,n_3} . dn_2 = 0$$

Rearranging the order of differentiation, this expression becomes

$$\left(\frac{\partial \mu_3}{\partial n_2}\right)_{n_1,n_3} = \left(\frac{\partial \mu_2}{\partial n_3}\right)_{n_1,n_2} = -\left(\frac{\partial \mu_2}{\partial n_2}\right)_{n_1,n_2} \cdot \left(\frac{dn_2}{dn_2}\right)_{n_1}$$

It will be seen that the expression $\left(\frac{dn_3}{dn_2}\right)_{n_1}$ will represent the intercept, at $n_2 = 1$, of a tangent drawn at any point to the curve of salt solubility plotted against salt-free binary composition x_2.

For salts exhibiting festoon-like solubility curves in a binary solvent, this intercept would be generally negative in value. When $\left(\frac{dn_3}{dn_2}\right)_{n_1}$ is negative, and since $\left(\frac{\partial \mu_3}{\partial n_3}\right)_{n_1,n_2}$ is inherently positive, it is seen from the above relation that μ_2 is an increasing function of salt concentration. When μ_2 is an increasing function of salt concentration, the Gibbs-Duhem equation indicates that μ_1 is a decreasing function of salt concentration. In other words, Component 2, the component in which the salt is less soluble, is salted out. Its increased chemical potential is manifested in its increased concentration in the vapor phase.

Nonelectrolyte Order

The electrostatic theories of salting out predict that the degree of salting out in aqueous solution increases with a decreasing dielectric constant of the nonelectrolyte.

For a given salt, it was observed that the value of the salting out parameter k_{32} was greater for alcohols of lower polarity. As the alcohol series is ascended and this component becomes less polar, it is observed to be more strongly salted out from aqueous solution by salts which cause this effect.

Order of Effectiveness of Salts

Salts have been ranked in their order of effectiveness previously by the value of the salting out parameter k_{32}.

The values of salt parameters reported in the Treatment of Results section are based on mole fraction salt concentrations. For highly electrovalent salts, salt order should be established by k values corrected for dissociation (i.e. by ionic strength). However, this would not apply for such salts as the mercuric halides. Therefore, a basis of comparison is difficult.

An average of the data listed in the literature[40] for salting out in solutions of two polar components yields the following diminishing average order:

cations : $Li - Na - K - Ba - NH_4 - Rb - Cs$
anions : $SO_4 - Cl - Br - NO_3 - I$

Examination of the experimental values of k_3, corrected for ionic strength, for various cations with each anion and for

various anions with each cation, in each binary system, yields the following diminishing average order:

cations : $Na - K - Pb - Ba - NH_4 - Hg$
anions : $SO_4 - Cl - Br - NO_3 - I$

This observed salt order is about as similar to the average order in the literature as any one from the investigations making up the average literature order. (It is to be emphasized that this latter order is very rough and changeable for polar solvents.)

Glasstone[57] lists the following crystallographic ionic radii:

Li	0.60	A.
Na	0.95	
Hg	1.10	
Pb	1.24	
K	1.33	
Ba	1.35	
NH_4	1.48	
Rb	1.48	
Cs	1.69	

The electrostatic theories of salt effect predict that salt effect diminishes with increasing ion radius, since the electrostatic field of the ions is greatest when ion radius is smallest, causing a maximum attraction for highly polar water molecules under this condition. However, it has been demonstrated previously that salt effect is not governed by electrostatic interaction alone but is rather a complex function of all possible interactions. This accounts for the fact that, although salting out generally diminishes in aqueous solution with increasing ion size, the order is not mirrored exactly. (The covalent nature of the mercuric halides accounts for the low effect of the relatively small mercuric ion).

SUMMARY

It is interesting to note that, for the systems investigated, this apparent balancing of various interactions enables this simple relation to represent not only the effect of the variation of salt concentration on the vapor-liquid equilibrium of a system for a single ratio of the two volatile components in the liquid phase, but also for any ratio of these two components, with a single value of k_3.

Salt effect in vapor-liquid equilibrium is proportional to the value of k_3, but is limited by salt solubility. The value of k_3 was found greatest for salts exhibiting the greatest solubility differences between the two components. However, the salt must be sufficiently soluble in the component in which it is less soluble, to dissolve to the concentration required for the separation. Both factors must be considered in the choice of a salt as an extractive agent.

Acknowledgment

The authors wish to acknowledge the National Research Council of Canada for their support in this investigation.

Nomenclature

Component 1 = water
,, 2 = alcohol
,, 3 = salt
n_i' = moles of component i in vapor phase
n_i = ,, ,, ,, ,, ,, liquid ,,
N_i = mole fraction component i in liquid (3 component basis)
x_i = ,, ,, ,, ,, ,, ,, (salt-free basis)
y_i = ,, ,, ,, ,, ,, ,,

$$y_1 = \frac{n_1'}{n_1' + n_2'} \qquad y_2 = \frac{n_2'}{n_1' + n_2'}$$

$$x_1 = \frac{n_1}{n_1 + n_2} \qquad x_2 = \frac{n_2}{n_1 + n_2}$$

$$N_3 = \frac{n_3}{n_1 + n_2 + n_3} \qquad S_3 = \frac{n_3}{n_1 + n_2}$$

T = temperature, °K
π = total pressure, atmospheres
P_i° = vapour pressure of pure component i at temperature in question
V_i = volume fraction component i in liquid (3 component basis)
R = gas constant
μ_i = chemical potential of component i
F_i° = free energy of component i in its standard state
C = empirical constant
γ_i = activity coefficient of component i
α = relative volatility

$$\gamma^i = \frac{y_i \pi}{P_i^\circ N_i} \qquad \alpha = \frac{y_2 x_1}{y_1 x_2}$$

References

(1) Jost, W., Chem.-Ing.-Tech. **23,** 64 (1951).
(2) Yamamoto, Y., et al, Chem. Eng. (Japan) **16,** 166 (1952).
(3) Samaddar, S. P., and Nandi, S. K., Trans. Indian Ch. E. **2,** 29 (1948-9).
(4) Bogart, M. J. P., and Brunjes, A. S., Chem. Eng. Progress **44,** 95 (1948).
(5) Bogart, M. J. P., and Brunjes, A. S., Chem. Abstr. **46,** 5084-W (1952).
(6) Fox, J. M., M.S. Thesis, University of Pennsylvania, Philadelphia, Pennsylvania (1949).
(7) Craven, E. C., Ind. Chemist **9,** 414 (1933).
(8) Guyer, A., Guyer, A. Jr., and Johnsen, B. K., Helv. Chem. Acta. **38,** 946 (1955).
(9) Butler, J. A. V., and Thompson, A., Proc. Roy. Soc. A141, 86 (1933).
(10) Butler, J. A. V., and Shaw, R., ibid A 129, 519 (1930).
(11) Costa Novella, E., and Tarraso, J. M., Anales real soc. espan. fis y. quim. (Madrid) **48B,** No. 6, 441 (1952).
(12) Googin, J. M., and Smith, H. A., Am. Chem. Soc. Meeting Abstr., Chicago, 61 R (Sept. 1953).
(13) Johnson, A. I., Ward, D. M., and Furtetr, W. F., Can. J. Technol. **34,** 429 (1957).
(14) Quartaroli, A., An. Chem. Applicata **33,** 141 (1943).
(15) Quartaroli, A., ibid **36,** 266 (1946).
(16) Quartaroli, A., ibid **36,** 273 (1946).
(17) Kyrides, L. P., et al, Ind. Eng. Chem. **24,** 795 (1932).
(18) Virtanen, A. I., and Pulkki, L., J. Am. Chem. Soc. **50,** 3138 (1928).
(19) Mariller, M., and Coutant, M., Bull. Assoc. Chem. Suc. Dist. France **42,** 288 (1925).
(20) Keyes, D. B., Ind. Eng. Chem. **33,** 1019 (1941).
(21) Sunier, A. A., and Rosenblum, C., Ind. Eng. Chem. Anal. Ed. **2,** 109 (1930).
(22) Walker, W. H., et al, "Principles of Chemical Engineering", 3rd Ed., McGraw-Hill, New York (1937).
(23) McBain, J. W., and Kam, J., J. Chem. Soc. **115,** 1332 (1919).
(24) Wright, R., J. Chem. Soc. **121,** 2251 (1922).
(25) Wright, R., ibid **123,** 2493 (1923).
(26) Wright, R., ibid **125,** 2068 (1924).
(27) Proszt, J., and Kollar, G., Hung. Tech. Abstr. 7, No. 1, 7 (1955).
(28) Proszt, J., and Kollar, G., Acta. Chim. Acad. Sci. Hung. 8, No. ¼, 171 (1955).
(29) Miller, W. L., J. Phys. Chem. **1,** 633 (1897).
(30) Gorhan, A., Internat. Sugar Jour. **35,** 266 (1933).
(31) Dittmar, H. F. L., Chem. Abstr. **45,** 1732-e (1951).
(32) Morrell, C. E., and Gilliland, E. R., U.S. 2,612,468 (30 Sept. 1952).
(33) Kelly, H. S., Jr., Chem. Abstr. **44,** 3245-d (1950).
(34) Garwin, L., and Hutchison, K. E., Ind. Eng. Chem. **42,** 727 (1950).
(35) Reider, R. M., and Thompson, A. R., ibid **42,** 379 (1950).
(36) Tursi, R. R., and Thompson, A. R., Chem. Eng. Progress **47,** 304 (1951).
(37) Fogg, E. T., Univ. Microfilms (Ann Arbor) Pub. No. 5589 (1953).
(38) Furter, W. F., Ph.D. Thesis, University of Toronto, Toronto, Ontario (1958).
(39) Gross, P., and Halpern, O., J. Chem. Phys. **2,** 184, 188 (1934).

(40) Long, F. A., and McDevit, W. F., Chem. Rev. **51,** 119 (1952).
(41) Debye, P., and McAuley, J., Physik Z. **26,** 22 (1925).
(42) Kirkwood, J. G., see reference 40 above.
(43) Altshuller, A. P., and Everson, H. E., J. Phys. Coll. Chem. **55,** 1368 (1951).
(44) Robinson, C. S., and Gilliland, E. R., "Elements of Fractional Distillation", 4th Ed., McGraw-Hill, New York (1950).
(45) Joseph, N. R., J. Biol. Chem. III, 481 (1935).
(46) Chu, J. C., et al, "Distillation Equilibrium Data", Reinhold Pub. Corp., New York (1950).
(47) Cornell, L. W., and Montanna, R. E., Ind. Eng. Chem. **25,** 1331 (1933).
(48) Doroszewsky, A., and Polansky, E., Z. Physik, Chem. **73,** 192 (1910).
(49) Gadwa, A., Ch.E. Thesis, Massachusetts Institute of Technology, Cambridge, Mass. (1936).
(50) Hughes, H. E., and Maloney, J. O., Chem. Eng. Progress **48,** 192 (1952).
(51) Johnson, A. I., and Furter, W. F., Can. J. Technol. **34,** 413 (1957).
(52) Othmer, D. F., and Benenati, R. F., Ind. Eng. Chem. **37,** 299 (1945).
(53) Perry, J. H., "Chemical Engineers' Handbook", 3rd Ed., McGraw-Hill, New York (1950).
(54) Uchida, S., and Kato, H., J. Soc. Chem. Ind. Japan **37,** 525 (1934).
(55) Seidell, A., "Solubilities of Inorganic and Metal Organic Compounds", 3rd Ed., D. Van Nostrand, New York (1940).
(56) Shemilt, L. W., Davies, J. A., and Gordon, A. R., J. Chem. Phys. **16,** 340 (1948).
(57) Glasstone, S., "Elements of Physical Chemistry", D. Van Nostrand, New York (1946).

★ ★ ★

ERRATUM:

An Analysis of Air and Solid Flow in a Spouted Wheat Bed by B. Thorley, J. K. Saunby, K. B. Mathur and G. L. Osberg, from the October 1959 issue.

On page 186, column 2, Equation (3) should read:

$$U_m = (D_p/D_c)(D_i/D_c)^{1/3}\left(2gL\frac{\rho_p-\rho_f}{\rho_f}\right)^{1/2} \quad \ldots\ldots\ldots(3)$$

instead of:

$$U_m' = (D_p/D_c)(D_i/D_c)^{1/3}\,2gL\left(\frac{\rho_p-\rho_f}{\rho_f}\right)^{1/2} \quad \ldots\ldots\ldots(3)$$

NOTE TO THE EDITOR

Solvent Extraction of Saskatchewan Lignites

II. Note on the Properties of the Extract[1]

S. D. CAVERS[2], R. L. EAGER[3] and J. H. HUDSON[4]

The extract obtained from Saskatchewan lignite[(1)] is a black, brittle, shiny solid, with a brown streak and a conchoidal fracture, similar in appearance to German montan wax. Table 1 compares properties of various extracts including one obtained from Saskatchewan lignite Sample 18[(1)] by grinding it to minus 0.5-in. and extracting it in 5.25-lb. batches at atmospheric pressure in Soxhlet apparatus with a mixture of 80 parts by volume of benzene and 20 of 95% ethanol[(2)]. When the solvent leaving the lignite was colorless the solution was filtered and the solvent evaporated. The yield was 2.5% (moisture-free basis). Table 1 shows that the Saskatchewan extract and a North Dakota extract are similar. Both have lower melting points and much higher resin contents than do the specimens from California and Germany.

The Sample 18 extract was examined in two commercial laboratories. One[(6)] attributed only slight waxy characteristics to the material and recommended against its further evaluation for use in polish. The other[(7)] reported 68% resin and 26% waxes in the extract but believed its commercial value to be small.

Attempts were made to increase the yield by acid treatment[(8,9)] both prior to and during extraction. Yields could be approximately doubled in both cases but consisted in part of a cinder-like solid which did not fuse on heating, but instead coked and charred. These results agree with those of others[(8)].

Since an increase in temperature of extraction can increase the yield of extract from lignite[(8)], Sample 18 was extracted at 77°C. with benzene-95% ethanol, 80:20 (b.p. 64°C. at 721mm.) with the apparatus pressurized[(10)]. Although an increased yield was obtained, the product was a rank-smelling, soft, black, sticky grease with no sharp melting point, and a resin content of 85%.

An attempt to decolorize extract from Sample 18 with activated charcoal (Norit Extra N) produced an orange gum almost wholly soluble in cold ether and therefore of high resin content.

The high resin content, low wax content, and low yield of the extract, combined with the failure of increased temperature of extraction, acid treatment, and activated charcoal treatment to produce a high quality extract, imply that the extraction of a wax is not likely to be feasible commercially.

References

(1) Eager, R. L., Cavers, S. D., Graham, W., Dunne, N. R., and Cudmore, W. J. G., Can. J. Technol. **34,** 121 (1956).
(2) Ode, W. H., and Selvig, W. A., Ind. Eng. Chem. **42,** 131 (1950).
(3) Abraham, H., "Asphalts and Allied Substances", Ed. V, Vol. II, 1074, D. Van Nostrand Co., New York (1945).
(4) Selvig, W. A., Ode, W. H., Parks, B. C., and O'Donnell, H. J., U.S Bur. Mines Bull. No. 482 (1950).
(5) De Angelis, F. J., American Lignite Products Co., Ione, Calif., Personal Communication, June 28, 1951.
(6) Whyte, D. E., S. C. Johnson and Son, Inc., Racine, Wis., Personal Communication, February 18, 1952.
(7) De Angelis, F. J., American Lignite Products Co., Ione, Calif., Personal Communication, April 14, 1952.
(8) Kiebler, M. W., Chapter 19 of "Chemistry of Coal Utilization", Vol. I (H. H. Lowry ed.), 685, 701, 702, John Wiley and Sons Inc., New York (1945).
(9) Grun, A., and Olbrick, E., Z. deut. 0l-u. Fett-Ind. **40,** 773 (1920), as reported in C.A. **15,** 744 (1921).
(10) De Witt, C. B., J. Chem. Educ. **8,** 1174 (1931).

[1]*Manuscript received and accepted March 14, 1960.*

[2]*Associate Professor, Department of Chemical Engineering, The University of British Columbia, Vancouver, B.C.*
[3]*Associate Professor, Department of Chemistry and Chemical Engineering, University of Saskatchewan, Saskatoon, Sask.*
[4]*Chemist, Saskatchewan Research Council, Saskatoon, Sask.*

Contribution from the Department of Chemistry and Chemical Engineering, University of Saskatchewan, Saskatoon, Sask. with financial assistance from the Saskatchewan Research Council.

TABLE 1
PROPERTIES OF EXTRACTS

	Raw Extract from Sample 18	Extract from a North Dakota Lignite (2,4)	Ione, Calif. Lignite Wax (5)	Raw California Lignite Wax (4)	Raw German Wax (4)
Solvent	Benzene, 95% ethanol, 80:20	Benzene, 95% ethanol, 80:20	–	Benzene, 95% ethanol, 80:20	–
Melting Point, °C.	74[a,d], 79[a,e]	73–77[c]	84[a]	80–86[c]	81–85[c]
Acid Value (4)	46[d]	54	44	67–76	27
Saponification Value (4)	108[d]	103	111	132–145	95
Ester Value (4)	62[d]	49	67	64–69	68
Specific Gravity 20°C./20°C.	1.06[d]	–	1.03	1.08–1.09	1.03
Resin (4)[b],%	71[d] at 10°C.	68	21	32–48	23

[a]Ring and ball method, A.S.T.M. Designation E28-42T (3).
[b]Solubility in cold ethyl ether.
[c]Closed capillary tube method (2,4).
[d]Figure refers to the product of an early run in the large Soxhlets.
[e]Figure refers to the mixed products of four runs in the large Soxhlets.

★ ★ ★

Polymeric Self-Sealing Distillation and Extractor Trays[1]

J. D. KILGALLON[2] and H. R. L. STREIGHT[2]

A suitable polymeric material offers several advantages over metals and alloys normally used for self-sealing or friction-fit trays in distillation and extraction columns, by reducing the capital cost and maintenance charges and by improving the efficiency of small diameter columns. The hydrophobic nature of polymeric materials also increases the plate efficiency of an extractor when the plate is wetted by a continuous organic phase which passes to a dispersed water phase.

The plate efficiency and performance of a small column are often reduced by leakage or by passing of vapor and liquor at the periphery of the trays. This problem can be overcome by using self-sealing polymeric trays arranged in cartridges which are assembled and inserted into the column shell as a unit. The flexible nature of polymers ensures a tight fit between the trays and the shell of the column, notwithstanding normal out-of-roundness of the shell.

A recent Canadian development is the Polymeric Self-Sealing Tray which may be used for distillation or extraction columns. Applications have been made for covering patents in Canada and other countries. The use of a suitable polymeric material (neoprene, polyethylene, Teflon polytetrafluoroethylene resin, a type of polyvinyl resin, etc.,) in a friction-fit type of tray offers advantages over metals and alloys both by reducing the capital cost and maintenance charges and by increasing the efficiency of a small column (24-in. diameter or less) particularly if operating with a low liquor rate. Polymeric materials are preferentially wetted by the organic phase in an extractor and give a greater plate efficiency than metals, provided water is the dispersed phase. Polymeric trays are also relatively cheap and easy to fabricate.

A distillation column normally consists of a vertical tubular shell containing a number of bubble cap, perforated or patented-types of trays. The plates or trays are held in place by the required number of support rings attached to the shell or by tie rods which pass through and hold the trays at the desired plate spacing. The tie rods of one tray are connected to the adjacent rods of the trays above and below. Pilot and commercial scale columns of this type are designed over a wide range of sizes, both in diameter and height.

Conventional perforated-trays have advantages over bubble cap-trays in distillation columns and extractors. The simplicity of construction, the greater capacity and the lower pressure drop are desirable characteristics of perforated-trays. The proposed polymeric trays are especially attractive if perforated although they are quite suitable for the attachment of bubble caps made of Teflon polytetrafluoroethylene resin, or other materials.

The bubble caps or perforations in a distillation plate or extractor act as a means for contacting vapor and liquid or a heavy liquid phase and a light liquid phase. The plate efficiency and performance of a column are decreased if vapor or liquid by-passes the contacting zone containing the bubble caps or the perforations and passes between the periphery of the plate and the shell. Usually vapor passes around the edge of a plate and liquid drops down the column wall as a falling film. Accordingly the plates should be sealed in a suitable manner against the inside surface of the enclosing shell to reduce or entirely prevent the leakage of vapor and liquid around the outer edges of the trays. This is especially true for a small diameter column as the plate-shell clearance exerts a greater effect on operation owing to the increased percentage free area.

Table 1 indicates common types of seals between trays and the associated methods of assembling the trays in the column.

Friction-fit trays are often preferred to other types of plates, especially in small diameter columns owing to their simplicity of assembly, low cost and the elimination of any problem associated with the selection of a suitable braided packing or gasket. An assembly of friction-fit plates can be quickly and accurately placed in a shell and firmly supported by metallic tie rods or support posts which slip or screw into neighbouring spacing members. The assembly enters the top of the shell-section and is removed from the bottom of the same section e.g., in the same direction from the top to the bottom of the column. In a small diameter column, there is a limited space for installing and removing the trays; peripheral packed or ring and gasket seals usually require shorter flanged sections of the column for tray assembly than friction-fit plates. Self-sealing trays also can be assembled in a shorter time.

Other sealing methods include the use of flexible polymeric gaskets which tightly enclose the outer edge of each plate or the addition of polymeric sealing ribbons which are fastened to the bottom edge of each tray. As the ribbon diameter is slightly greater than the column diameter, the ribbon tilts upward against the shell as the plate is drawn into the column. Thus there is a close fit between the ribbon or packing material and the shell.

Metallic friction-fit trays often permit excessive by-passing of vapor and liquor at the plate-shell interface, particularly if the diameter of the column is less than 30 inches. Gaps occur between the metallic plate and the shell owing to normal out-of-roundness of the shell and the plate and because of permanent deflections of the lip, formed during assembly. When a standard metallic tray enters a column which is not perfectly round, the lip of the tray may be deflected by interference sufficiently to introduce a permanent set on the lip which prevents the lip

[1]*Manuscript received November 13, 1959; accepted March 15, 1960.*
[2]*Du Pont of Canada Limited, Montreal, Que.*
Based on a paper presented at the C.I.C. Chemical Engineering Conference, Hamilton, Ont., November 9-11, 1959.

TABLE 1
SEALS AND ASSEMBLY OF TRAYS IN A COLUMN

Method	Description of Seal	Assembly of Tray	Range
Peripheral Packed	A gland forces and clamps a braided packing between the shell and a packing ring, attached to the tray.	A complete tray or sections of a tray are assembled inside the column.	Column diameter >30 in.
Ring and Gasket	An angle iron or ring attached to the shell supports the sections of each tray. The seal is made by a gasket and held in place by studs, etc.	Individual trays are inserted and assembled inside the column.	Column diameter >30 in.
Friction-fit	The edge of each tray is lifted by pressing, rolling or flaring until the lip will rest against the shell.	For small diameter columns, assemble a cartridge or a number of trays united by the tie rods at the correct plate spacing; each cartridge is drawn into the shell and fastened to an adjacent cartridge by means of the tie rods. For larger columns, the trays can be inserted one at a time and fixed by the tie rods.	Any diameter

from sealing when it reaches its ultimate position. However, polymeric trays are unusually resilient, fit tightly against the shell of the column and deflect liquid from the periphery on to the trays.

Nature of the Plate Efficiency

The efficiency of a perforated-plate column extractor is affected by the physical characteristics of the fluid system, flow rates, tray design and also by the wetting properties of the material selected for the plates. Garner and his associates[1] have examined the literature and verified by experiments in a 4-in. perforated-plate extractor that the nature of the trays will alter the plate efficiency in a predictable manner.

For efficient operation, Garner has shown that the droplets should have regular size and shape at the plate surface or the plates should be preferentially wetted by the continuous phase. As Teflon and to a slighter extent polyethylene are preferentially wetted by a continuous organic phase, plate efficiency is increased if such polymers are used for the plates provided the water phase is dispersed and the direction of mass transfer is from the continuous organic phase to the dispersed water phase. Thus for effective aqueous phase dispersion, the plate surface must be hydrophobic in nature and be preferentially wetted by the continuous organic solvent phase. Tests made by Garner showed Teflon polytetrafluoroethylene resin and polyethylene are strongly hydrophobic and metals are more hydrophilic. The experimental runs were made on two systems, having a dispersed water phase. The tests showed that the plate efficiency was increased by approximately 30% and 12% when mild steel was replaced by the above polymers, the higher value being obtained on the system with the greater interfacial tension. Mild steel plates gave a larger hold up on the plates and blobs of liquid, instead of a continuous stream of relatively small droplets of fairly uniform size, as noted for polymeric plates.

When the organic solvent phase is dispersed in an aqueous continuous phase, a metal plate was found to be slightly better than a polymeric plate because a metal is preferentially wetted by a continuous aqueous phase. Brass or clean mild steel is better than rusted mild steel which lies about halfway in wettability between brass and Teflon.

Mechanical Design

The object of this development is to provide a tray for use in fluid contacting equipment which possesses self-sealing characteristics by virtue of its shape and of the material from which it is constructed. The mechanical details of the proposed tray for a distillation column are shown in Figure 1 and for an extractor in Figure 2. Arrangements for a distillation column are equally applicable for an extractor and vice versa. The polymeric tray can be given additional rigidity by adding reinforcing rings as illustrated for an extractor in Figure 2 or by reinforcing the polymer with asbestos or Fiberglas, etc. The new Teflon X-100 moulding resins particularly lend themselves to tray fabrication insofar as reinforcing ribs and weirs can be moulded directly into the tray.

In the drawings, the shell of the distillation column is marked as (1) and the polymeric plate with turned up lip as (2) and (3) respectively. The tie rods may be joined as in (4) by screwing one rod into the other or as in (5) by inserting one rod into another. A typical tubular downcomer or upcomer is shown as (6) and a typical set of perforations as (7). The upper and lower reinforcing rings, (8) and (9) respectively, are held together by the nut and bolt assembly marked as (10).

Figure 1 presents a plan and a cross-sectional view of a distillation column. The weir, (11), can be welded directly to the tray or secured to the tray by means of studs and nuts or pegs. The downcomer consists of a solid moulding and nut, (12), made of the same polymeric material as the tray. The nut is fitted from underneath the tray and tightened to keep the downcomer in position. An upcomer can be secured in a similar manner.

The supporting rings are useful to reduce or eliminate sagging of a large plastic tray. The material selected for the top and bottom metal plates will depend on the nature of the process materials in the column. The shape of the cut-out and the unsupported area of the plate can vary with the particular process. Additional rigidity can also be obtained by adding reinforcing ribs on one or both sides of the tray.

It is clear from the drawings that the polymeric self-sealing plate is of simple construction. The flange at the edge of the plate provides simple and secure sealing between that plate and the shell of the column. The height of the flange, the angle at which it meets the plate and the thickness of the tray may be varied to meet the requirements of design. A laminated lip may be used to guarantee a reduction of by-pass vapor and/or liquor. The proposed polymeric plate permits unit construction, convenient installation and removal.

The polymeric material is chosen on the basis of its resistance to chemical attack, non-tendency to swell, and on the temperature and pressure conditions within the column. Teflon polytetrafluoroethylene resin is usually preferred to other materials as it is more rigid and does not have the tendency to swell and buckle in the presence of many solvents. The maximum service temperature for Teflon polytetrafluoroethylene resin is about 300°C. and for the majority of other polymers only about 80°C. Any flanged plates supporting the polymeric tray should be of a material substantially chemically and physically inert to the chemicals with which they will come in contact.

Installation

Two operating columns containing polymeric self-sealing trays, 10 and 12 inches in diameter, have provided the required separation without mechanical trouble. The actual capacities were found to be lower than expected as the orifice coefficient

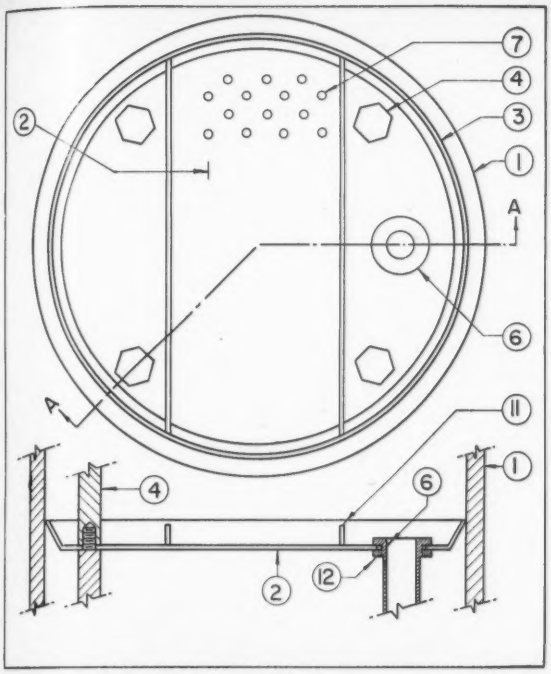

Figure 1—Polymeric self-sealing distillation tray. Plan and cross-section, A-A.

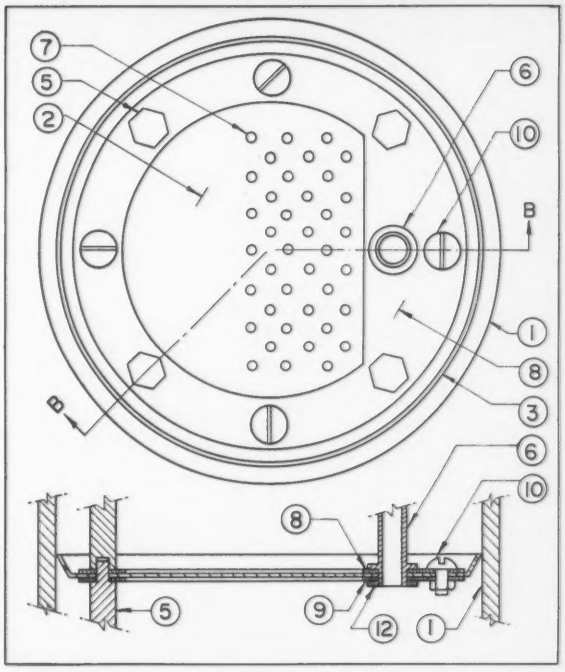

Figure 2—Reinforced polymeric self-sealing extractor tray. Plan and cross-section, B-B.

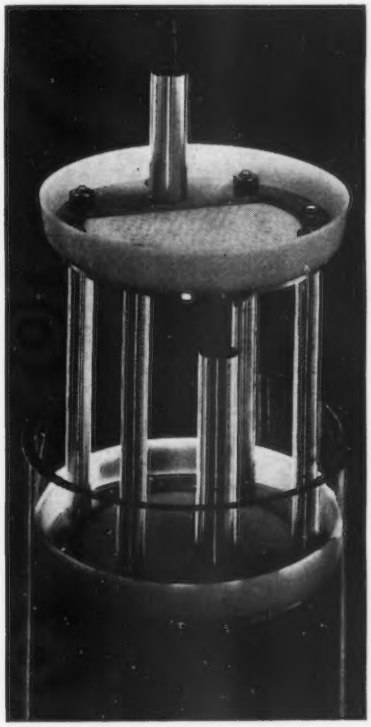

Figure 3—Demonstration model of two polymeric trays partly inserted in shell.

that was used during the design was found to be too high. Based on our experience, the orifice coefficient should be determined for the polymer selected for the trays. Polymers differ from metals in wettability and compressibility; the holes might decrease slightly in size after drilling and not be of the same shape. The capacities of the two columns were increased to the designed throughputs after the number of holes were enlarged in accordance with the corrected orifice coefficient.

Fabrication of Polymeric Trays

The plates being used at present were manufactured by Joseph Robb and Co. Limited of Montreal. The various steps in the manufacture of the polymeric material are as follows:

No. 5 Teflon polytetrafluoroethylene powder, with a bulk factor of 4 to 1, is thoroughly screened and loaded into a steel frame mounted on a press with top and bottom pads of Masonite. The powder is then compressed for ten minutes at a pressure of 2,000 lb./sq. in ga. The biscuit, as it is now called, is then removed from the frame and the edges trimmed, at which point it is placed in the oven and the temperature elevated to 385°C. The curing cycle is approximately one hour for 1/8 in. thick sheet, sized 36 in. × 36 in. and a half hour for $\frac{1}{16}$ in. thickness. In the oven the material is transposed from the powder to the jell state. It is removed from the oven and put into a press for twenty minutes at a pressure of 1000 lb./sq. in. ga. The resulting sheet is now Teflon polytetrafluoroethylene resin in its common form. Sheets of Teflon are cut into discs which are placed in steel ring moulds to form a tray of a given size. The trays are put in the press and the temperature is elevated approximately to 65°C. for five minutes after which the trays of Teflon are removed, trimmed and drilled to give a finished product as is illustrated in Figure 3, a photograph of a demonstration model made by Joseph Robb and Co. Limited.

Conclusion

The proposed polymeric trays seem particularly suitable for small diameter distillation columns and for extractors in which water is the dispersed phase. The advantages of assembly and improved operation should contribute to the acceptance and use of polymeric trays in distillation and extraction columns.

References

(1) Garner, F. H., Ellis, S. R. M. and Hill, J. W., A.I.Ch.E.J., **1**, 185 (1955) and Trans. Instn. Chem. Engrs., **34**, 223 (1956).

★ ★ ★